

Polishing the Lens: I Pionic Final State Interactions and HBT Correlations-Distorted Wave Emission Function (DWEF) Formalism and Examples

Gerald A. Miller and John G. Cramer
 Department of Physics, University of Washington
 Seattle, WA 98195-1560

The effects of interactions of pions emitted from a dense system of matter are incorporated using an optical potential formalism. The need for replacing the plane wave pions of earlier approaches by “distorted waves” computed using an optical potential is explained, and the constraining influence of chiral symmetry on the optical potential is discussed. The new HBT formalism, DWEF, which incorporates the distorted waves is derived and implemented in a practical manner suitable for numerical calculations. The STAR Au+Au pionic data (at $\sqrt{s} = 200$ GeV) for HBT correlations and the spectrum is studied for three different regions of centrality, with good agreement. Furthermore, the influence of the real part of the optical potential is found to be crucial: this potential is so deeply attractive that the pions can be said to be massless inside the medium. Predictions are made for central Cu+Cu collisions (at $\sqrt{s} = 200$ GeV). The squares of pionic distorted wave functions, obtained as exact numerical solutions to the wave equation, are displayed and significant differences with the results of using the familiar eikonal approximation are found. Using the eikonal approximation leads to a qualitative accounting for the effects of the imaginary part of the optical potential, but fails entirely to include the effects of the real part of the optical potential. A simple example is used to illustrate that an attractive optical potential can have large effects on extracting radii and can also lead to oscillations in radii measured at low momenta. We also show that a commonly used smoothness approximation is not valid for pions of low momenta, but works very well if the average pion momentum is greater than about 160 MeV/c.

I. INTRODUCTION

Measurements of the two-particle momentum correlations between pairs of identical particles have been used to study the space-time structure of the “fireball” produced in the collision between two heavy ions moving relativistically. The quantum statistical effects of symmetrization cause an enhancement of the two-boson coincidence rate at small momentum differences that can be related to the space-time extent of the particle source. This method, called HBT interferometry, has been applied extensively in recent experiments at the Relativistic Heavy Ion Collider (RHIC) by the STAR and PHENIX collaborations. See the reviews[1, 2, 3, 4].

The invariant ratio of the cross section for the production of two pions of momenta $\mathbf{p}_1, \mathbf{p}_2$ to the product of single particle production cross sections is analyzed as the correlation function $C(\mathbf{p}_1, \mathbf{p}_2)$. We define $\mathbf{q}=\mathbf{p}_1-\mathbf{p}_2$ and $\mathbf{K}=(\mathbf{p}_1+\mathbf{p}_2)/2$, with \mathbf{K}_T as the component perpendicular to the beam direction. (We focus on mid-rapidity data, where $\mathbf{K} = \mathbf{K}_T$.) The correlation function can be parameterized for small \mathbf{q} as $C(\mathbf{q}, \mathbf{K}) - 1 \approx \lambda \exp(-R_O^2 q_O^2 - R_S^2 q_S^2 - R_L^2 q_L^2) \approx \lambda(1 - R_O^2 q_O^2 - R_S^2 q_S^2 - R_L^2 q_L^2)$ ($q_i R_i \ll 1$), where O, S, L represent directions parallel to \mathbf{K}_T , perpendicular to \mathbf{K}_T and the beam direction, and parallel to the beam direction[5]. Early [6] and recent [3] hydrodynamic calculations predicted that a fireball evolving through a quark-gluon-hadronic phase transitions would emit pions over a long time period, causing a large ratio R_O/R_S . The puzzling experimental result that $R_O/R_S \approx 1$ [7] is part of what has been called “the RHIC HBT puzzle” [8].

Another part of the puzzle is that the measured radii depend strongly on the average momentum K , typically decreasing in size by about 50% over the measured range. This dependence of a geometrical parameter on the probe momentum shows immediately that the radii are not simply a property of a static source. The influence of the interactions between the pionic probe and the medium, as well as the effects of transverse flow, must be taken into account when extracting the radii. The medium at RHIC seems to be a very high density, strongly interacting plasma[9], so that any pions made in its interior would be expected to interact strongly.

We studied the effects of including the pionic interactions in previous work[10], finding that the only way to simultaneously describe the measured HBT radii and pionic spectra is to include the effects of pion-medium final state interactions by solving the relevant relativistic wave equation. These interactions are so strongly attractive that the pions act as essentially massless objects inside the medium. The medium acts as if it is free

of the chiral condensate that is the source of the pion mass, and therefore acts as a system with a restored chiral symmetry.

The principal aim of the present work is to present a detailed treatment of the formalism that will allow wide application of our technique, and we present some new applications here. We also provide specific simple examples to demonstrate that the effects of pionic interactions cause the measured sizes of the medium to be different than the true sizes. Furthermore, we shall explicitly demonstrate that classical treatments of the pion-medium interactions, based on using the eikonal approximation for solutions of the wave equation are not valid. In addition, we are able to demonstrate that the commonly used smoothness approximation is not valid at low momenta (<200 MeV/c).

An outline of the remainder of this paper follows. Previous standard formalisms that use plane wave pions are briefly reviewed in Sect. II. The technical method of incorporating the influence of final state interactions between the pion and the medium is described in Sect. III. Pionic emission in the absence of final state interaction is described with an emission function S_0 that is of a form motivated by hydrodynamics. The connection between the symmetries of this function (for the case of head-on collisions) and the form of the pion optical potential is described in Sect. IV. The role of the complex optical potential is explained in Sect. V, and the specific numerical algorithm necessary for its incorporation is presented in Sect. VI. Once our approach is defined, there is only one approximation we need to make. The validity of this requires only that the source size be much larger than the inverse of the temperature. This large source approximation, LSA, is explained in Sect. VII. The resulting distorted wave emission function, DWEF, is evaluated using two different equivalent methods in Sec. VIII. This section also extends earlier numerical results[10] by computing the dependence of the HBT radii and pionic spectra on the centrality in Au+Au collisions and by making predictions for Cu+Cu central collisions. The eikonal approximation to solving the wave equation is discussed in Sect. IX in which the importance influence of the opacity and the vanishing of the effects of the real potential are also described. The role of chiral symmetry [34] in constraining the form of the optical potential for low energies is discussed in Sect. X. The importance of the real part of the optical potential in obtaining oscillating radii at low energies is illustrated through two examples in Sect. XI. The commonly used “smoothness approximation” is studied in Sect. XII. A brief summary is presented in Sect. XIII. Finally, a short appendix verifies an approximation to an integral.

II. PREVIOUS FORMALISM – PLANE WAVE PIONS

The aim is to include the effects of final state interactions of outgoing pions. We’ll begin with a brief review of the formalism previously used to describe HBT correlations for situations in which the pions do not interact with the medium.

The relevant observables are the covariant single- and two-particle emission functions defined as appropriately normalized ratios of cross sections[11]

$$\mathcal{P}_1(\mathbf{p}) = E \frac{1}{\sigma} \frac{d\sigma_\pi}{d^3\mathbf{p}} \quad (1)$$

$$\mathcal{P}_2(\mathbf{p}_1, \mathbf{p}_2) = E_1 E_2 \frac{1}{\sigma} \frac{d\sigma_{\pi\pi}}{d^3\mathbf{p}_1 d^3\mathbf{p}_2} \quad (2)$$

$$\int \frac{d^3p}{E} \mathcal{P}_1(\mathbf{p}) = \langle N \rangle \quad (3)$$

$$\int \frac{d^3p_1}{E_1} \frac{d^3p_2}{E_2} \mathcal{P}_2(\mathbf{p}_1, \mathbf{p}_2) = \langle N(N-1) \rangle \quad (4)$$

$$C(\mathbf{p}_1, \mathbf{p}_2) = \frac{\langle N \rangle^2}{\langle N(N-1) \rangle} \frac{\mathcal{P}_2(\mathbf{p}_1, \mathbf{p}_2)}{\mathcal{P}_1(\mathbf{p}_1)\mathcal{P}_1(\mathbf{p}_2)} \rightarrow \frac{\mathcal{P}_2(\mathbf{p}_1, \mathbf{p}_2)}{\mathcal{P}_1(\mathbf{p}_1)\mathcal{P}_1(\mathbf{p}_2)}. \quad (5)$$

The last step of Eq. (5) is obtained because $\langle N^2 \rangle \gg \langle N \rangle$ for the very high energy collisions of interest here.

These observables can be expressed in terms of an emission function $S(x, K)$ that is the Wigner transform of the density matrix associated with assumed classical currents which emit the pions. The literature [11] presents the emission function as

$$S_0(x, K) = \int \frac{d^4y}{2(2\pi)^3} \exp(-iK \cdot y) \langle J^*(x+y/2) J(x-y/2) \rangle, \quad (6)$$

where the brackets indicate an ensemble average. In the following we assume that the emission process is initially uncorrelated: the pions are emitted from chaotic sources that have random phases[11, 12]. This assumption seems consistent with analysis of data produced at SPS and RHIC[4]

Our use of the subscript 0 denotes that the effects of final state interactions are ignored. In this plane wave (pw) approximation, the observables can be expressed as

$$P_1^{pw}(\mathbf{p}) = \int d^4x S_0(x, p), \quad p_0 = \omega_p \equiv \sqrt{\mathbf{p}^2 + m_\pi^2}, \quad (7)$$

$$C_0(\mathbf{p}_1, \mathbf{p}_2) \equiv C_0(\mathbf{q}, \mathbf{K}) = 1 + \frac{|\int d^4x S_0(x, K) e^{-iq \cdot x}|^2}{\int d^4x S_0(x, p_1) \int d^4x S_0(x, p_2)}, \quad (8)$$

$$q = p_1 - p_2, \quad K = \frac{1}{2}(p_1 + p_2). \quad (9)$$

The HBT radii are characterized in two different ways that are equivalent in principle. In the first method, one treats the momentum differences $q_{O,S,L}$ as small quantities and then expands keeping terms to second order so that:

$$C(q, K) - 1 \approx 1 - q_O^2 R_O^2 - q_S^2 R_S^2 - q_L^2 R_L^2, \quad (10)$$

where q_O is the transverse component that is parallel to the direction of \mathbf{K} , q_S is the transverse component that is perpendicular to the direction of \mathbf{K} , and q_L is the longitudinal component. Another parametrization is

$$C(q, K) - 1 \approx \exp(-q_O^2 R_O^2 - q_S^2 R_S^2 - q_L^2 R_L^2), \quad (11)$$

As stated above, the correlation function (8) is obtained assuming that the sources are incoherent. In practice, describing data and extracting radii require using:

$$C(q, K) - 1 \approx \lambda \exp(-q_O^2 R_O^2 - q_S^2 R_S^2 - q_L^2 R_L^2), \quad (12)$$

$$C(q, K) - 1 \approx \lambda(1 - q_O^2 R_O^2 - q_S^2 R_S^2 - q_L^2 R_L^2), \quad (13)$$

in which λ is typically about 1/2. The vitiating factor λ is the fraction of the pairs that originate from the space-time region relevant for correlations, see the review [4]. Current understanding [4] is that the HBT data are consistent with incoherent emission, and accounting for the many pions that are produced by the decays of resonances far outside the collision region can reproduce the factor λ . These pions are not correlated with the pions emitted from the produced hot dense matter but can't be separated from those that are.

The influence of resonances affects the extraction of radii and the measurements of the pionic spectrum differently. We account for this in our phenomenological analysis, see the erratum of Ref. [10].

The approximate forms (12,13) provide two ways to extract radii. The former suggests that

$$R_i^2 = \frac{1}{q_i^2} \ln \frac{\lambda}{C(q_i, K) - 1}, \quad i = O, S, L \quad (14)$$

while the latter implies

$$R_i^2 = \frac{1}{q_i^2} \frac{C(q_i, K) - 1}{\lambda}, \quad i = O, S, L \quad (15)$$

Eq. (14) can be used for values of q_i such that $(C - 1)/\lambda$ can be approximated by a Gaussian function. The use of Eq. (15) requires that $q_i R_i \ll 1$.

A final comment concerns the smoothness approximation which is to replace the momenta p_1, p_2 appearing in Eq. (8) by K . In this case, and assuming the validity of Eq. (15) the squared radii are moments of the emission function S_0 . The application of the moment formalism therefore requires that $q_i R_i \ll 1$.

III. FINAL STATE INTERACTIONS

The above formalism envisions a pionic wave equation of the generic form

$$\left(\frac{\partial^2}{\partial t^2} - \nabla^2 + m_\pi^2 \right) \phi = J, \quad (16)$$

with J as the source of pions. Here and throughout the paper we use natural units in which \hbar and c are unity. This equation may be re-expressed in terms of the Green's function G_0 :

$$G_0^{-1}\phi = J \quad (17)$$

with the subscript 0 indicating that no final state interactions are included. Note that the quantity that enters the relevant S -matrix elements is J . We wish to include the effect that an escaping pion has to "fight" its way through the medium. The effects of the fighting distort the wave. These interactions of the pions with the medium, represented by the optical potential U , lead to a modified equation

$$\left(\frac{\partial^2}{\partial t^2} - \nabla^2 + U + m_\pi^2\right)\phi = J, \quad (18)$$

or using the complete Green's function G , we have

$$G^{-1}\phi = J. \quad (19)$$

But G and G_0 are related by the equation:

$$G = G_0 + G_0UG = G_0(1 + TG_0), \quad (20)$$

so that the quantity $G_0^{-1}\phi$ is replaced by $G_0^{-1}GJ$. The second equality of (20) defines the T the scattering matrix that sums the effects of the interactions U : $T = U(1 + G_0T)$. In coordinate space the factor $1 + TG_0$ is the complex conjugate of the incoming wave function, so that the formal result can be expressed simply[11]: The outgoing plane wave factors (*e.g.* $e^{ip_1 \cdot x_1}$) of (8) and (6) should be replaced by the full scattering wave function $\psi_{\mathbf{p}_1}^{(-)*}(x_1)$ [11], so that

$$J(x) \rightarrow J(x)\psi_{\mathbf{p}}^{(-)*}(x)e^{-ip \cdot x} \quad (21)$$

We assume that U (and therefore $\psi_p^{(-)}(x)$) is independent of the final state. If the source has many pions this approximation should be good. Thus

$$S(x, p_1) = \int \frac{d^4y}{2(2\pi)^3} \langle J^*(x + y/2)J(x - y/2) \rangle \psi_{\mathbf{p}_1}^{(-)}(x + y/2)\psi_{\mathbf{p}_1}^{(-)*}(x - y/2), \quad (22)$$

which applies for calculating the single-particle emission function and

$$S(x, K, q) = \int \frac{d^4y}{2(2\pi)^3} \langle J^*(x + y/2)J(x - y/2) \rangle \psi_{\mathbf{p}_1}^{(-)}(x + y/2)\psi_{\mathbf{p}_2}^{(-)*}(x - y/2), \quad (23)$$

which applies for calculating the two-particle emission function. In the plane wave limit, $S(K, q) \rightarrow S_0(K)e^{-iq \cdot x}$.

Physical observables for the emission of two pions of momenta p_1, p_2 are determined by the correlation function $C(q, K)$ ($K = \frac{1}{2}(p_1 + p_2)$, $q = p_1 - p_2$) which is given by

$$C(q, K) = 1 + \frac{|\int d^4x S(x, K, q)|^2}{\int d^4x S(x, p_1) \int d^4x S(x, p_2)}. \quad (24)$$

One obtains the usual expression (8) if the wave functions $\psi_{\mathbf{p}}^{(-)}$ are replaced by plane wave functions ($\psi_{\mathbf{p}}^{(-)}(x) \rightarrow e^{-ip \cdot x}$). The smoothness approximation to the correlation function is obtained if one replaces the momenta $p_{1,2}$ appearing in the denominator of Eq. (24) by K . This involves some ambiguity because it is not numerically true that $K^0 = \sqrt{\mathbf{K}^2 + m_\pi^2}$ because K is an average momentum. (For \mathbf{q} in the S or L direction $|\mathbf{p}_1| = |\mathbf{p}_2|$ and the four-vector $K^2 = m_\pi^2$. For \mathbf{q} in the O direction $K^2 = m_\pi^2 + q_O^2 \frac{K_T^2}{\omega(K_T)^2}$. This is very close to m_π^2 if $q_O^2 \ll m_\pi^2$ or K_T is small. The advantage of using the smoothness approximation is that radii can be obtained as moments of the emission function if the using the quadratic approximation to the correlation function is allowed. Therefore results of this procedure can be compared with experimental data only if the values of $q_{L,O,S}R_{L,O,S} \ll 1$.)

The expression (23) contains the ensemble average of the currents. This may be expressed in terms of $S_0(x, K)$ by taking the Fourier transform of Eq. (6). We then obtain the convolution formula:

$$S(x, K, q) = \int d^4K' S_0(x, K') \int \frac{d^4y}{(2\pi)^4} e^{iK' \cdot y} \psi_{\mathbf{p}_1}^{(-)}(x + y/2)\psi_{\mathbf{p}_2}^{(-)*}(x - y/2), \quad (25)$$

where the subscripts indicate the momenta p_1, p_2 of the detected pions and $K = \frac{1}{2}(p_1 + p_2)$. The quantity $S(x, K, q)$ is used to compute experimental observables in the same way that S_0 was previously used. This is the distorted wave emission function DWEF formalism. We emphasize that S_0 (which reflects the true properties of the source) is no longer directly related to observables— the appearance of distorted waves obscures the relationship between the data and the true properties of the source. The expression (25) is implied by the formalism of Ref. [11].

IV. SYMMETRIES OF $S_0(x, K)$ AND THE FORM OF THE PION DISTORTED WAVES

We use the hydrodynamic parameterization of the source of Ref. [13, 14, 15]. Generally based on the Bjorken tube model, it is given by

$$S_0(x, K) d^4x = \frac{M_\perp \cosh(\eta - Y)}{(2\pi)^3} \frac{1}{\exp\left[\frac{(K \cdot u(x) - \mu_\pi)}{T(x)}\right] - 1} \rho(b) \exp\left[-\frac{(\eta - \eta_0)^2}{2(\Delta\eta)^2}\right] \\ \times \tau d\tau \left[\frac{1}{\sqrt{2\pi(\Delta\tau)^2}} \exp\left(-\frac{(\tau - \tau_0)^2}{2(\Delta\tau)^2}\right) \right] d\eta b db d\phi, \quad (26)$$

$$d^4x = \tau d\tau d\eta b db d\phi. \quad (27)$$

Here, μ_π is the pion chemical potential, the variables $(b, \phi) = \mathbf{b}$ are equivalent to \mathbf{x}_\perp , $\eta = \frac{1}{2} \ln \frac{t+z}{t-z}$, $\tau = \sqrt{t^2 - z^2}$, $M_T = \sqrt{K_\perp^2 + m_\pi^2}$, $Y = \frac{1}{2} \ln \frac{E_K + K_z}{E_K - K_z}$. The factor in the brackets involving τ has the same normalization as the delta function: $\delta(\tau - \tau_0)$. We use a Bose-Einstein distribution instead of the Boltzmann distribution of Ref. [15] and also allow the transverse density $\rho(b)$ to have a general form instead of a Gaussian.

We concentrate on the kinematics of the STAR experiment which detects pions within half a unit of rapidity of moving perpendicular to the beam, so we take $Y = 0$. This means that the average momentum is transverse: $\mathbf{K} = \mathbf{K}_\perp = \mathbf{K}_T$. With colliding beams of equal mass and energy there is a fore-aft symmetry along the longitudinal axis, so that we use $\eta_0 = 0$. The parameterization (26) is motivated by hydrodynamical models with approximately boost-invariant longitudinal dynamics. It uses thermodynamic and hydrodynamic parameters and appropriate coordinates. The “emission function” given above was originally intended to parameterize the distribution of points of last interaction in the source. In conventional treatments, the Cooper-Frye[16] matching procedure is used to obtain distributions of detected particles. Our approach is different. We assume that pions can be formed at any space-time point during the collision, but propagate through the dense medium while interacting before being detected. Thus we take $S_0(x, K)$ to be the emission function in the absence of final state interactions.

The velocity field $u(x)$ describing the dynamics of the expanding source is parameterized by [17]

$$u^\mu(x) = (\cosh \eta \cosh \eta_t(b), \cos \phi \sinh \eta_t(b), \sin \phi \sinh \eta_t(b), \sinh \eta \cosh \eta_t(b)), \quad (28)$$

with ϕ the angle between \mathbf{K}_\perp and \mathbf{u} (or when appearing in the single-particle emission function, it is the angle between \mathbf{p}_i and \mathbf{u}). Eq. (28) implements a boost-invariant longitudinal flow profile $v_L = z/t$, with a linear radial profile of strength η_f for the transverse flow rapidity:

$$\eta_t(b) = \eta_f \frac{b}{R}. \quad (29)$$

The exponent that enters in the Bose-Einstein distribution is given by the four-vector dot product:

$$K \cdot u(x) = M_\perp \cosh(\eta - Y) \cosh \eta_t(b) - K_\perp \sinh \eta_t(b) \cos \phi. \quad (30)$$

The presence of a non-vanishing value of η_f causes the emission function to depend on both K and M_\perp .

Note that the model contains the parameters: $R, \eta_0, \Delta\eta, \Delta\tau, \tau_0, \eta_f$. As stated originally, temperature gradients were included, but we treat the temperature as a constant for our numerical calculations. We shall see below that our formalism can easily be generalized to allow the temperature to vary as a function of b .

The longitudinal η, τ and transverse (\mathbf{b}, \mathbf{K}) variables can be separated in the following form:

$$S_0(x, K) = S_0(\eta, \tau) B_\eta(\mathbf{b}, \mathbf{K}) \quad (31)$$

$$B_\eta(\mathbf{b}, \mathbf{K}) \equiv \frac{M_\perp}{\exp[(K \cdot u - \mu_\pi)/T] - 1} \rho(b) \quad (32)$$

$$\mathcal{S}_0(\eta, \tau) \equiv \frac{\cosh(\eta - Y)}{(2\pi)^3} \exp\left[-\frac{\eta^2}{2(\Delta\eta)^2}\right] \frac{1}{\sqrt{2\pi(\Delta\tau)^2}} \exp\left[-\frac{(\tau - \tau_0)^2}{2(\Delta\tau)^2}\right]. \quad (33)$$

Here $\rho(b)$ is a function, normalized as $\rho(0) = 1$ that represents the transverse density. Conditions for the STAR detector correspond to values of Y near 0.

The Bose-Einstein distribution of Eq. (32) is evaluated as a sum of Boltzmann distributions:

$$\frac{1}{\exp\left[\frac{K \cdot u(x) - \mu_\pi}{T}\right] - 1} = \sum_{n=1}^{\infty} \exp\left(\frac{-K \cdot u + \mu_\pi}{T_n}\right), \quad T_n \equiv \frac{T}{n}. \quad (34)$$

We note that the emission function of Eq. (26) has been previously used in the “blast-wave model” [18], and we would like to comment on the differences between our formalism and that model. These include:

- The blast-wave model does not attempt to reproduce the normalization of the spectrum, and sets the chemical potential μ_π to 0. We find that μ_π is fairly large, and affects both the normalization and the *shape* of the pion momentum spectrum.
- The blast-wave model uses the smoothness approximation (see Sect. XII) and computes HBT radii as moments of the emission function. We find that these approximations are not valid below about 160 MeV/c and lead to somewhat different radii even at higher momenta.
- The blast-wave model uses plane waves and therefore omits the effects of the optical potential.

V. FINAL STATE INTERACTIONS AND THE OPTICAL POTENTIAL

The salient feature of the 200 GeV data is the high density of the produced matter, so we treat the effects of pion final state interactions with a dense medium. We adopt a single-channel approach that uses the interaction-distorted incoming wave $\Psi_{\mathbf{p}_1}^{(-)*}(x_1)$.

We assume that the matter formed in the central region of the collision is cylindrically symmetric with a very long axis, so that an expression of the form (31) is valid. In that case, the optical potential U representing the interaction between a pion and the medium is a complex, azimuthally-symmetric function depending on pion momentum and local density. Within our formalism the influence of some time-dependent effects in U introduced by the time-dependent source S_0 is incorporated in the energy dependence of the optical potential, and the pion-medium interaction time is restricted by S_0 .

The optical potential accounts for the interaction between each pion and the surrounding medium, but does not include the interaction between the two pions. In particular, the Coulomb interaction is known to be important. The experimental analysis removes this effect before extracting radii from the data. The Coulomb interaction between pions is of long range and exists outside the medium, while the optical potential acts only when pions are inside. We therefore expect that presence of the optical potential would not influence the removal of the Coulomb interaction.

The optical potential accounts for situations in which the pion changes energy or disappears entirely due to its interactions with the dense medium. We do not assume to know the content of the dense medium, and therefore will use a phenomenological optical potential. But it is worthwhile to consider a simple example to get an idea about how large the optical potential can be. Suppose, *e.g.*, that the medium is a gas of pions. Then $\pi\pi$ scattering would be the origin of U . In the impulse approximation, the central optical potential would be $U_0 = -4\pi f \rho_0$, where f is the complex forward scattering amplitude and ρ_0 the central density. For low energy pion-pion interactions, $4\pi \text{Im}[f(p)] = p\sigma$, with $\sigma \approx 1$ mb. At a momentum $p = 1 \text{ fm}^{-1} = 197.3 \text{ MeV}/c$, using a pion density about ten times the baryon density of ordinary nuclear matter, $\text{Im}[U(0)] \approx -0.15 \text{ fm}^{-2}$, representing significant opacity.

The optical potential must be an analytic function of energy, and therefore the existence of an imaginary part mandates the existence of a real part. Thus, any analysis needs to treat U as a complex function. Under certain circumstances the real part can be very large. For example, if two interacting pions each have less energy than half of the rho meson mass, the final state interactions caused by virtual transitions to a rho meson would be strongly attractive. Additionally, the influence of chiral symmetry restoration can lead to a strong real part.

We shall discuss the phenomenological forms and theories of the optical potential in subsequent sections. For now we simply proceed using the assumption that U is a complex, azimuthally-symmetric function depending on pion momentum and local density.

VI. FINDING $\psi^{(\pm)}(\mathbf{x})$

The evaluation of the emission function (25) requires performing an eight dimensional integral using a distorted wave. We shall use symmetries to reduce the number of numerical evaluations. Doing this depends on obtaining a compact expression for the distorted wave. In the present section, we show how the distorted waves are evaluated.

The first step is to realize that the function $\psi_{\mathbf{p}}^{(-)}(x)$ represents an energy-eigenfunction[11]. So we have

$$\psi_{\mathbf{p}}^{(-)}(x) = e^{-i\omega_p x^0} \Psi_{\mathbf{p}}^{(-)}(\mathbf{x}). \quad (35)$$

To proceed we need to examine the properties of the wave function $\psi_{\mathbf{p}}^{(-)}(\mathbf{x})$. It is conventional to compute $\psi_{\mathbf{p}}^{(+)}(\mathbf{x})$, and we will follow this convention. However, one may use time reversal invariance in the form

$$\Psi_{\mathbf{p}}^{(-)}(\mathbf{x}) = \Psi_{-\mathbf{p}}^{(+)*}(\mathbf{x}) \quad (36)$$

to obtain the desired wave function.

The next step is to realize that for central collisions, $Y = 0$, the emission function (33) has a cylindrical symmetry. This means that expected optical potential is azimuthally symmetric. If we take the matter to have the form of a very long tube, the optical potential will be independent of z . Then one obtains a solution that takes a product form

$$\Psi_{\mathbf{p}_{1,2}}^{(-)}(\mathbf{x}) = e^{\mp i q_L z/2} \psi_{\mathbf{p}_{1,2}}^{(-)}(\mathbf{x}_{\perp} = \mathbf{b}), \quad (37)$$

$$\mathbf{p}_{1,2} = \mathbf{K} \pm \mathbf{q}/2 \pm \hat{\mathbf{z}} q_L/2, \quad (38)$$

with by definition \mathbf{q} is a transverse vector $\mathbf{q} \cdot \hat{\mathbf{z}} = 0$.

We may obtain the wave function $\psi_{\mathbf{p}}^{(+)}(\mathbf{b})$ by solving the wave equation

$$(-\nabla_{\perp}^2 + U(b)) \psi_{\mathbf{p}}^{(-)*}(\mathbf{b}) = p^2 \psi_{\mathbf{p}}^{(-)*}(\mathbf{b}). \quad (39)$$

If $U = 0$, $\psi_{\mathbf{p}}^{(+)}(\mathbf{b}) = e^{i\mathbf{p} \cdot \mathbf{b}}$. Many previous treatments of opacity can be understood as using the eikonal approximation to obtain solutions to Eq. (39).

We take

$$U(b) = U_0(p)\rho(b) + U_1(p)\nabla\rho \cdot \nabla, \quad (40)$$

where $U_{0,1}$ are complex numbers depending on the pion momentum $p = |\mathbf{p}|$, and $\rho(b)$ is any well-behaved function which falls to 0 as $b \rightarrow \infty$. The second term (of the Kisslinger form[19]) enters if the pionic scattering is in a p-wave. Further discussion about the optical potential and its relation to chiral symmetry restoration is to be found in Sects. VIII B and X.

Given (40) the solution for $\psi_{\mathbf{p}}^{(\pm)}(\mathbf{b})$ can be expanded in partial wave form in plane polar coordinates ($b \equiv \sqrt{\mathbf{x}_{\perp}^2}$, ϕ , $\cos \phi \equiv \hat{\mathbf{p}} \cdot \hat{\mathbf{b}}$):

$$\psi_{\mathbf{p}}^{(+)}(\mathbf{b}) = \sum_{m=-\infty, \infty} f_m(p, b) i^m e^{im\phi}, \quad (41)$$

$$\psi_{\mathbf{p}}^{(+)}(\mathbf{b}) = f_0(p, b) + 2 \sum_{m=1, \infty} f_m(p, b) i^m \cos m\phi, \quad (42)$$

with (42) taking into account the invariance of the differential equation for f_m under the interchange $b \rightarrow -b$. Note that we may use Eq. (36) to find

$$\psi_{\mathbf{p}}^{(-)*}(\mathbf{x}_{\perp}) = f_0(p, b) + 2 \sum_{m=1, \infty} f_m(p, b) (-i)^m \cos m\phi. \quad (43)$$

In practice a finite number of terms is needed, with $m \leq m_{max} \approx 2pR/\hbar$.

Use Eq. (42) in (39) to find

$$\left(\frac{d^2}{db^2} + \frac{1}{b} \frac{d}{db} + \left(p^2 - \frac{m^2}{b^2} \right) \right) f_m(p, b) - U \left(\frac{b^2}{R^2} \right) f_m(p, b) = 0. \quad (44)$$

Note that for large enough b , U vanishes and the f_m are linear combinations of Bessel J_m and Neumann N_m functions or Hankel functions $H_m^{(1,2)}$.

This differential equation can be solved numerically using the Runge-Kutta technique. One determines the wave function, by matching the numerical solutions to the analytic solution

$$f_m(p, b) = A_m \left(J_m(pb) + T_m H_m^{(1)}(pb) \right). \quad (45)$$

One matches the numerical function and its derivative (at large enough b so that $U = 0$) so as to determine the constants A_m, T_m . The normalization of $\psi_{\mathbf{p}}^{(\pm)}$ is such that $A_m = 1$ —asymptotically the wave is a sum of an ordinary plane wave and an outgoing wave, and the functions $f_m(p, b)$ can be regarded as phase shifted Bessel functions. Using the partial-wave form of two-dimensional wave function (42) will simplify the evaluation of $S(x, K)$ of Eq. (25).

VII. THE DISTORTED WAVE EMISSION FUNCTION (DWEF) AND THE LARGE SOURCE APPROXIMATION (LSA)

Using (35) in Eq.(25) allows the integrals over y^0 and $K^{0'}$ to be evaluated as:

$$S(x, K, q) = \int \frac{d^3 K'}{(2\pi)^3} S_0(x; K^0, \mathbf{K}') e^{i(\omega_2 - \omega_1)x^0} \int d^3 y e^{-i\mathbf{K}' \cdot \mathbf{y}} \Psi_{\mathbf{p}_1}^{(-)}(\mathbf{x} + \mathbf{y}/2) \Psi_{\mathbf{p}_2}^{(-)*}(\mathbf{x} - \mathbf{y}/2), \quad (46)$$

and using (38) allows the integrals over y^3 and $K^{3'}$ to be evaluated yielding a four-dimensional integral:

$$S(x, K, q) = \frac{1}{(2\pi)^2} S_0(\tau, \eta) e^{iq^0 t - iq_1 z} \int d^2 b' \tilde{B}_\eta(\mathbf{b}, \mathbf{b}') \psi_{\mathbf{p}_1}^{(-)}(\mathbf{b} + \mathbf{b}'/2) \psi_{\mathbf{p}_2}^{(-)*}(\mathbf{b} - \mathbf{b}'/2), \quad (47)$$

$$\tilde{B}_\eta(\mathbf{b}, \mathbf{b}') \equiv \int d^2 K'_T B_\eta(\mathbf{b}, \mathbf{K}'_T) \exp[-i\mathbf{K}'_T \cdot \mathbf{b}'].$$

The result (47) still requires the evaluation of an 6-dimensional integral (over $\tau, \eta, \mathbf{b}', \mathbf{K}'_T$) to obtain the correlation function. We search for simplifications. The integral (47) simplifies if we ignore the effects of transverse flow rapidity. So to gain insight, let's set

$$\eta_f = 0, \quad (48)$$

consider a fixed value of η , and take one of the terms in the series (34). Then

$$\tilde{B}_\eta(\mathbf{b}, \mathbf{b}') = \rho(b) g(\mathbf{b}'^2) \quad (49)$$

$$g(\mathbf{b}'^2) = 2 \int d^2 K_\perp M_\perp \exp \left[\frac{-M_\perp \cosh \eta}{T} \right] \exp[-i\mathbf{K}_\perp \cdot \mathbf{b}'] \quad (50)$$

Fig. 1 shows $g(b)$ for the case $T/\cosh \eta = m_\pi$. It is clear from (50) that the quantity T controls the range of allowed values of K_\perp , so that the extent of b' is of order $1/T \approx 1$ fm for $T = 200$ MeV. This is much smaller than the size of the presumed fireball that controls the extent of b in (47). Thus it is natural to think of neglecting the terms involving $\pm \mathbf{b}'/2$ of (47). This however, is too extreme an approximation because it would not lead to the formalism of Sect. 1 in the plane wave limit. Instead, we use the approximation

$$\psi^{(-)}(\mathbf{b} \pm \mathbf{b}'/2) \approx e^{\mp i\mathbf{p}_\perp \cdot \mathbf{b}'/2} \psi^{(-)}(\mathbf{b}) \quad (51)$$

This is exact in the plane wave limit, but its wider validity relies on the replacement

$$\psi_{\mathbf{p}_i}^{(-)}(\mathbf{b} + \mathbf{b}'/2) \psi_{\mathbf{p}_j}^{(-)*}(\mathbf{b} - \mathbf{b}'/2) g(\mathbf{b}'^2) \approx \psi_{\mathbf{p}_i}^{(-)}(\mathbf{b}) \psi_{\mathbf{p}_j}^{(-)*}(\mathbf{b}) g(\mathbf{b}'^2) \exp(i\mathbf{K}_\perp \cdot \mathbf{b}'), \quad (52)$$

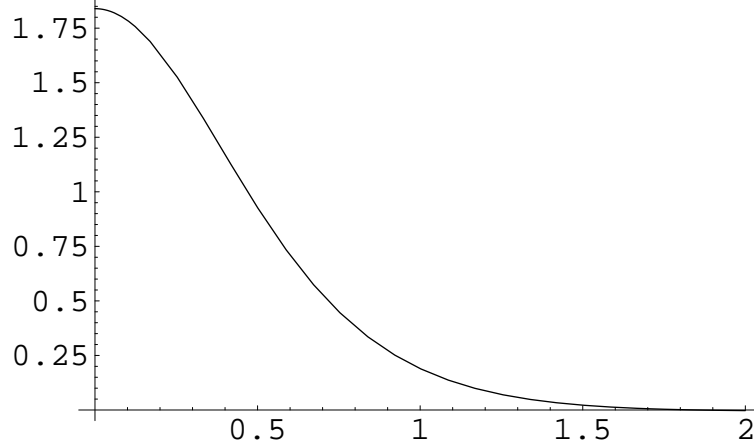


FIG. 1: Plot of $g(b)$, showing cutoff around $b = 1/T$, with $T = 1/m_\pi$ and b in fm.

that requires only that the size of the source be much larger than T^{-1} . We use this “Large Source Approximation” (LSA) to immediately integrate over \mathbf{b}' and to obtain a simpler version of (47):

$$S(x, K) = S_0(\tau, \eta, Y = 0) e^{i(\omega_2 - \omega_1)\tau \cosh \eta} e^{-iq_L \tau \sinh \eta} B_\eta(\mathbf{b}, \mathbf{K}) \psi_{\mathbf{p}_1}^{(-)}(\mathbf{b}) \psi_{\mathbf{p}_2}^{(-)*}(\mathbf{b}), \quad (53)$$

that is obtained for *any* value of η_f . The expansion (34) gives

$$\begin{aligned} B_\eta(\mathbf{b}, \mathbf{K}) &= \sum_{n=1}^{\infty} \exp\left(\frac{-K \cdot u + \mu_\pi}{T_n}\right) M_T \rho(b) \\ &= \sum_{n=1}^{\infty} \exp\left(\frac{-M_T \cosh \eta \cosh \eta_t(b) + \mu_\pi}{T_n}\right) \exp\left(\frac{K_T \sinh \eta_t(b) \cos \phi}{T_n}\right) M_T \rho(b), \end{aligned} \quad (54)$$

so that Eq. (53) becomes

$$S(x, K, q) = S_0(\tau, \eta) e^{i(\omega_2 - \omega_1)\tau \cosh \eta} e^{-iq_L \tau \sinh \eta} \sum_{n=1}^{\infty} \exp(-\gamma_n(b) \cosh \eta) B_n(\mathbf{b}, \mathbf{K}) \psi_{\mathbf{p}_1}^{(-)}(\mathbf{b}) \psi_{\mathbf{p}_2}^{(-)*}(\mathbf{b}) \quad (55)$$

$$B_n(\mathbf{b}, \mathbf{K}) \equiv \exp(\mu_\pi/T_n) \exp(K \sinh \eta_t(b) \cos \phi/T_n) M_T \rho(b) \quad (56)$$

$$S(x, p_i) = S_0(\tau, \eta) \sum_{n=1}^{\infty} \exp(-\gamma_n(b) \cosh \eta) B_n(\mathbf{b}, \mathbf{p}_i) \left| \psi_{\mathbf{p}_i}^{(-)}(\mathbf{b}) \right|^2, \quad (57)$$

$$\gamma_n(b) \equiv \frac{M_T \cosh \eta_t(b)}{T_n}. \quad (58)$$

The number of terms in the summation over n required to achieve an accurate result depends on the values of μ_π, \mathbf{K} . If desired the quantities T, μ_π can be treated as functions of b [13] in Eq. (56).

VIII. CORRELATION FUNCTION

The specific form of the wave function enables us to express the correlation function as $C(q_L \hat{\mathbf{z}} + \mathbf{q}, \mathbf{K})$:

$$C(q_L \hat{\mathbf{z}} + \mathbf{q}, \mathbf{K}) = 1 + \frac{|\int d^4x S(x, K, q)|^2}{\int d^4x S(x, p_1) \int d^4x S(x, p_2)} \quad (59)$$

$$\mathbf{p}_{1,2} = \mathbf{K} \pm q_L/2\hat{\mathbf{z}} \pm \mathbf{q}/2. \quad (60)$$

The dependence on q_L occurs only in the numerator.

The remaining task is to perform the integral over d^4x . We use two separate approaches. The first employed is in [10] involves expanding $S(x, K)$, Eq. (56), as double power series in q_L and τ , keeping all terms up to second order. The second involves exact numerical integration. The two methods yield nearly identical results, with the second being more accurate and taking only slightly more computer time. We present both methods here. First, we take \mathbf{q} to be small and make expansions Sec. VIII A. This formalism is applied to obtain numerical results for radii and spectra in Sects. VIII B, VIII C and Sect. VIII D. The formalism to compute the correlation functions without the use of expansion is contained in Sec. VIII E, and this formalism is applied to compute correlation functions in Sec. VIII F.

A. Evaluation of correlation function by expansion

Now we make the above mentioned expansion keeping terms to order q_L^2 , (and anticipate the integration over η, τ). The term linear in q_L is an odd function of η so that it vanishes the integration over η is carried out. Use $\omega_2 - \omega_1 = -q_o\beta, \beta \equiv K_T/M_T$. Thus the expansion of Eq. (56) is

$$S(x, K) = S_0(\tau, \eta) \left(1 - iq_o\beta\tau \cosh \eta - \frac{1}{2}q_o^2\beta^2\tau^2 \cosh^2 \eta - \frac{1}{2}q_L^2\tau^2 \sinh^2 \eta \right) \times \sum_{n=1}^{\infty} \exp(-\gamma_n(b) \cosh \eta) B_n(\mathbf{b}, \mathbf{K}_T) \psi_{\mathbf{p}_1}^{(-)}(\mathbf{b}) \psi_{\mathbf{p}_2}^{(-)*}(\mathbf{b}), \quad (61)$$

The next step in evaluating (59) is to integrate over all τ, η using the measure $d\eta\tau d\tau$. The first integral to appear arises from the factor of unity appearing inside the parenthesis of (61). It is

$$I_0 \equiv \frac{1}{\sqrt{2\pi}\Delta\tau} \int_{-\infty}^{\infty} d\eta \cosh \eta \int_{-\infty}^{\infty} \tau d\tau \exp\left(-\frac{\eta^2}{2(\Delta\eta)^2}\right) \exp\left(-\frac{(\tau - \tau_0)^2}{2(\Delta\tau)^2}\right) \exp(-\gamma_n(b) \cosh \eta) \approx 2\tau_0 \exp\left(\frac{1}{\Delta\eta^2}\right) K_1\left(\gamma_n + \frac{1}{\Delta\eta^2}\right) \equiv \tau_0 f_0(\xi_n) \exp\left(\frac{1}{\Delta\eta^2}\right), \quad f_0(\xi_n) = 2K_1(\xi_n), \quad \xi_n \equiv \gamma_n + \frac{1}{\Delta\eta^2}. \quad (62)$$

The approximation involves the replacement

$$\exp\left(-\frac{\eta^2}{2(\Delta\eta)^2}\right) \rightarrow \exp\left(\frac{1}{\Delta\eta^2}\right) \exp\left(-\frac{1}{\Delta\eta^2} \cosh \eta\right). \quad (63)$$

Similar replacements are made below. The dominant contributions to the integral involve small values of η , so the approximation is expected to be very good. The appendix shows that the error involved is less than about 2%.

We proceed to use the same replacement to evaluate the remaining integrals and find

$$I_2 \equiv \frac{1}{\sqrt{2\pi}\Delta\tau} \int_{-\infty}^{\infty} \cosh \eta d\eta \int_{-\infty}^{\infty} \tau d\tau \exp\left(-\frac{\eta^2}{2(\Delta\eta)^2}\right) \exp\left(-\frac{(\tau - \tau_0)^2}{2(\Delta\tau)^2}\right) \exp(-\gamma_n(b) \cosh \eta) (-iq_o\beta)\tau \cosh \eta \approx (-iq_o\beta)(\tau_0^2 + (\Delta\tau)^2) \exp\left(\frac{1}{\Delta\eta^2}\right) f_2(\xi_n), \quad f_2(\xi_n) = K_0(\xi_n) + K_2(\xi_n) = 2\left(K_0(\xi_n) + \frac{K_1(\xi_n)}{\xi_n}\right), \quad (64)$$

$$I_3 \equiv \frac{1}{\sqrt{2\pi}\Delta\tau} \int_{-\infty}^{\infty} \cosh \eta d\eta \int_{-\infty}^{\infty} \tau d\tau \exp\left(-\frac{\eta^2}{2(\Delta\eta)^2}\right) \exp\left(-\frac{(\tau - \tau_0)^2}{2(\Delta\tau)^2}\right) \exp(-\gamma_n(b) \cosh \eta) (q_o\beta)^2 \tau^2 \cosh^2 \eta \approx (3\tau_0\Delta\tau^2 + \tau_0^3)(q_o\beta)^2 \exp\left(\frac{1}{\Delta\eta^2}\right) f_3(\xi_n), \quad f_3(\xi_n) = 2\frac{K_2(\xi_n)}{\xi_n} = 2\left(K_0(\xi_n)/\xi_n + K_1(\xi_n)\left(1 + \frac{2}{\xi_n^2}\right)\right), \quad (65)$$

$$I_1 \equiv \frac{1}{\sqrt{2\pi}\Delta\tau} \int_{-\infty}^{\infty} d\eta \cosh \eta \int_{-\infty}^{\infty} \tau d\tau \exp\left(-\frac{\eta^2}{2(\Delta\eta)^2}\right) \exp\left(-\frac{(\tau - \tau_0)^2}{2(\Delta\tau)^2}\right) \exp(-\gamma_n(b) \cosh \eta) \tau^2 \sinh^2 \eta \approx \tau_0(3\Delta\tau^2 + \tau_0^2) \exp\left(\frac{1}{\Delta\eta^2}\right) f_1(\xi_n), \quad f_1(\xi_n) = 2(K_2(\xi_n)/\xi_n) = 2K_0(\xi_n)/\xi_n + 4K_1(\xi_n)/\xi_n^2. \quad (66)$$

Then

$$\int d^4x S(x, K, q) = \tau_0 \exp\left(\frac{1}{\Delta\eta^2}\right) \times \left[\Phi_{12} - iq_o\beta(\tau_0 + \Delta\tau^2/\tau_0)F_2(K_T) - \frac{1}{2}q_o^2\beta^2(3\Delta\tau^2 + \tau_0^2)F_3(K_T) - q_L^2/2F_1(K_T) \right], \quad (67)$$

where

$$\Phi_{12} = \sum_{n=1}^{\infty} \int d^2b f_0(\xi_n) B_n(\mathbf{b}, \mathbf{K}_T) \psi_{\mathbf{p}_1}^{(-)}(\mathbf{b}) \psi_{\mathbf{p}_2}^{(-)*}(\mathbf{b}) \quad (68)$$

$$F_2(K_T) = \sum_{n=1}^{\infty} \int d^2b f_2(\xi_n) B_n(\mathbf{b}, \mathbf{K}_T) |\psi_{K_T}^{(-)}(\mathbf{b})|^2 \quad (69)$$

$$F_3(K_T) = \sum_{n=1}^{\infty} \int d^2b f_3(\xi_n) B_n(\mathbf{b}, \mathbf{K}_T) |\psi_{K_T}^{(-)}(\mathbf{b})|^2 \quad (70)$$

$$F_1(K_T) = \sum_{n=1}^{\infty} \int d^2b f_1(\xi_n) B_n(\mathbf{b}, \mathbf{K}_T) |\psi_{K_T}^{(-)}(\mathbf{b})|^2 \quad (71)$$

The denominator is obtained by evaluating the emission function (58) and the following functions enter:

$$F_0(K_T) = \sum_{n=1}^{\infty} \int d^2b f_0(\xi_n) B_n(\mathbf{b}, \mathbf{K}_T) |\psi_{K_T}^{(-)}(\mathbf{b})|^2 \quad (72)$$

$$\Phi_{ii} = \sum_{n=1}^{\infty} \int d^2b f_0(\xi_n) B_n(\mathbf{b}, \mathbf{K}_T) |\psi_{\mathbf{p}_i}^{(-)}(\mathbf{b})|^2. \quad (73)$$

With these definitions, one may show:

$$C(\mathbf{q} + q_L \hat{\mathbf{z}}, \mathbf{K}_T) = 1 - q_l^2 R_l^2 - q_o^2 \beta^2 \widetilde{\Delta\tau}^2 + \frac{|\Phi_{12}|^2}{\Phi_{11} \Phi_{22}} \quad (74)$$

$$R_l^2 = (3\Delta\tau^2 + \tau_0^2) F_1(K_T) / F_0(K_T) \quad (75)$$

$$\widetilde{\Delta\tau}^2 = (3\Delta\tau^2 + \tau_0^2) F_3(K_T) / F_0(K_T) - (\tau_0 + \Delta\tau^2 / \tau_0)^2 \left| \frac{F_2(K_T)}{F_0(K_T)} \right|^2. \quad (76)$$

The spectra are given by Eq. (3) [2]

$$E_p \frac{dN}{d^3p} = \frac{dN}{dY M_{\perp} dM_{\perp} d\phi_p} = \int d^4x S(x, p), \quad (77)$$

so that in general

$$\frac{dN}{dM_{\perp}^2} = \frac{1}{2} (2\pi) \int dY \int d^4x S(x, p), \quad (78)$$

in which the azimuthal symmetry of the angular distribution is used.

The STAR detector receives pions for values of Y between ± 0.5 and presents its results in terms of $\langle \frac{dN}{2\pi M_{\perp} dM_{\perp} dY} \rangle_{|Y| < 0.5}$ which is given by

$$\left\langle \frac{dN}{2\pi M_{\perp} dM_{\perp} dY} \right\rangle = \int_{-0.5}^{0.5} dY \int d^4x S(x, K). \quad (79)$$

Numerical studies showed us that the integration over Y is extremely well approximated by simply replacing Y by 0. Thus we find

$$\left\langle \frac{dN}{2\pi M_{\perp} dM_{\perp} dY} \right\rangle_{|Y| < 0.5} \cong \frac{\tau_0}{8\pi^3} \exp\left(\frac{1}{\Delta\eta^2}\right) F_0(\mathbf{K}_T). \quad (80)$$

The evaluation proceeds by reducing the two dimensional integrals of Eqs. (68-73) to those of one dimension by an analytic evaluation of the angular integrals. We need the partial wave expansions

$$\psi_{\mathbf{p}_1}^{(-)*}(\mathbf{b}) = f_0(p_1, b) + 2 \sum_{m=1, \infty} f_m(p_1, b) (-i)^m \cos m\phi_1 \quad (81)$$

$$\psi_{\mathbf{p}_2}^{(-)}(\mathbf{b}) = f_0^*(p_2, b) + 2 \sum_{m=1, \infty} f_m^*(p_2, b) (i)^m \cos m\phi_2, \quad (82)$$

where $\cos \phi_i = \widehat{\mathbf{p}}_i \cdot \widehat{\mathbf{b}}$.

We encounter integrals of the form

$$A_{mn}(z) = \int_0^{2\pi} d\phi e^{z \cos \phi} \cos m\phi_1 \cos n\phi_2. \quad (83)$$

For $\mathbf{q} \parallel \mathbf{K}$, $\mathbf{q} = \mathbf{q}_o$, $\phi_1 = \phi_2 = \phi$, so that we define

$$A_{mn}(\parallel, z) \equiv \int_0^{2\pi} d\phi e^{z \cos \phi} \cos m\phi \cos n\phi \quad (84)$$

$$= \pi (I_{m+n}(z) + I_{m-n}(z)), \quad (85)$$

where $I_{m\pm n}(z)$ are modified Bessel functions:

$$I_n(z) = (-i)^n J_n(iz), \quad (86)$$

for real z , and $I_n(z) = I_{-n}(z)$. An integral representation is

$$I_n(z) = \frac{1}{2\pi} \int_0^{2\pi} d\phi e^{z \cos \phi} \cos n\phi. \quad (87)$$

For $\mathbf{q} \cdot \mathbf{K} = 0$, $\mathbf{q} = \mathbf{q}_s$, we define

$$\cos \alpha = \frac{K}{\sqrt{K^2 + q^2/4}}, \quad \sin \alpha = \frac{q/2}{\sqrt{K^2 + q^2/4}}. \quad (88)$$

Then

$$A_{mn}(\perp, z) = \pi (I_{m+n}(z) \cos(m-n)\alpha + I_{m-n}(z) \cos(m+n)\alpha). \quad (89)$$

Note that for the denominators, one gets integrals in which the two angles of (83) are the same. Then the expression (85) is to be used.

The use of (85) and (89) in (55) yields

$$\begin{aligned} \Phi_{12}(\parallel, \perp) &= M_{\perp}(K) \int_0^{\infty} bdb\rho(b) e^{-M_{\perp}(K) \cosh \eta_t(b)/T} \\ &\times \left[\sum_{m,n=0}^{\infty} \epsilon_m \epsilon_n f_m(p_1, b) f_n^*(p_2, b) (i)^{n-m} A_{mn}(\parallel, \perp, \frac{K}{T} \sinh \eta_t(b)) \right] \end{aligned} \quad (90)$$

$$\epsilon_0 = 1, \quad \epsilon_{n>0} = 2. \quad (91)$$

The notation (\parallel, \perp) denotes either of the two possibilities $\mathbf{q} \parallel \mathbf{K}, \mathbf{q} \perp \mathbf{K}$. Similarly,

$$\begin{aligned} \Phi_{ii}(\parallel, \perp) &= M_{\perp}(p_i) \int_0^{\infty} bdb\rho(b) e^{-M_{\perp}(p_i) \cosh \eta_t(b)/T} \\ &\times \left[\sum_{m,n=0}^{\infty} \epsilon_m \epsilon_n f_m(p_i, b) f_n^*(p_i, b) (i)^{n-m} A_{mn}(\parallel, \perp, K \sinh \eta_t(b)/T) \right] \end{aligned} \quad (92)$$

B. Central Au+Au Collisions

The description of the formalism is essentially complete. A brief discussion of the phenomenology needed to define out theory is necessary prior to presenting the numerical results. The function $\rho(b)$ represents the cylindrically symmetric transverse source density and appears in the bare emission function S_0 and in the optical potential. We use

$$\rho(b) = [1/(\exp((r - R_{WS})/a_{WS}) + 1)]^2, \quad (93)$$

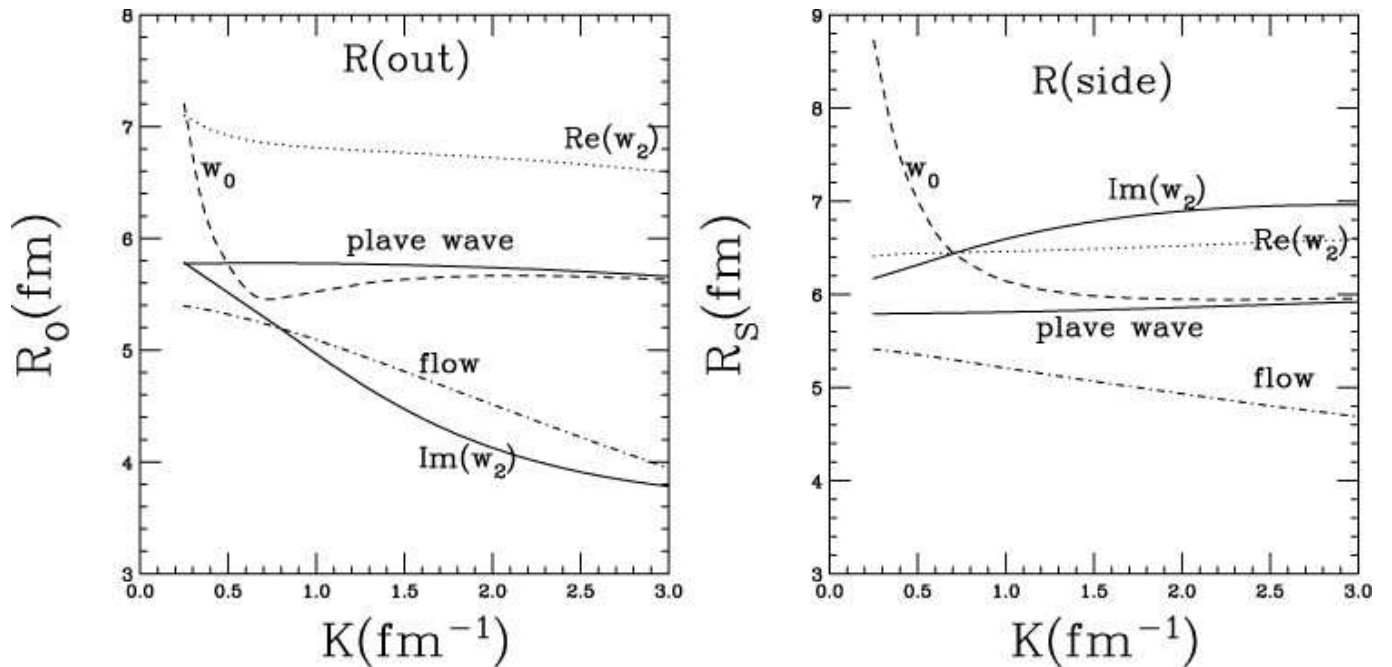


FIG. 2: Calculations of R_o and R_s ; Solid: plane wave (PW) calculation with $w_0 = 0, w_2, \eta_f = 0$; dash DWEF: $w_0 = 0.15 \text{ fm}^{-2}, w_2, \eta_f = 0$; dot DWEF: $w_2 = 0.3, W_0, \eta_f = 0$; dot-dash PW: $\eta_f = 1, w_0, w_2 = 0$; solid DWEF $w_2 = 0.15i, w_0, \eta_f = 0$. Effects of time duration are ignored here.

reflecting superimposed nuclear densities. The transverse flow rapidity is treated as a linear radial profile of strength η_f :

$$\eta_t(b) = \eta_f \frac{b}{R_{WS}}. \quad (94)$$

Next we discuss our phenomenology of the optical potential. The general forms are discussed in Eqs. (40,133). We find for the 200 GeV data, that the results prefer a small value of the gradient terms of those equations. Thus the optical potential is modeled as:

$$U_p(b) = -(w_0 + w_2 p^2) \rho(b), \quad (95)$$

with w_0 real (no opacity at $p=0$). The density profile $\rho(b)$ is that specified in $S_0(x, K)$. This simple form is sufficient to account for the data we study, $K_T \leq 600 \text{ MeV}/c$, but the interaction really does not grow as p^2 for p much greater than about 400 MeV/c.

The formalism of Sect. VIII and the equations of the present section define our model. Our technique may be compared with the Buda-Lund model, an efficient representation of the data[20], in which the temperature and fugacity are taken as position-dependent functions appearing in a Boltzmann distribution. The effects of our optical potential could provide an explanation of some of those deduced dependencies.

We show the parameters of the erratum of Ref. [10], see Table 1. These were obtained for Au+Au central collisions at 200 GeV. The quadratic forms (13,15) were used to obtain radii.

We assess the importance of the various effects for computing the radii R_O, R_S in Fig. 2. The curves labeled plane wave are computed using plane wave pion wave functions and setting the flow parameter $\eta_f = 0$. Then terms $w_0 = 0.15 \text{ fm}^{-2}$ corresponding to a well depth of $.15/(2m_\pi) = 15 \text{ MeV}$, $w_2 = 0.30$ corresponding to 30 MeV at $K = 1 \text{ fm}^{-1}$, and $w_2 = 0.15i$ are used. The flow $\eta_f = 1$ is used with $w_{0,2} = 0$. The other parameters are as in Table 1. We see that substantial effects are expected even with modest values of the parameters.

The next step is to use the parameters of Table 1 to reproduce the (corrected) results of that paper. These results are displayed here for completeness and to serve as reference points for discussions presented below. As shown in Figs. 3,4, the data [21, 22] are described very well indeed. It is worthwhile to describe our present treatment of the spectrum. We need to remove the effects of pions originating from weak decays and from decays of resonances. These pions are produced far outside the source region, and do not contribute to the Bose-Einstein enhancement. We therefore modified the measured spectrum by removing the 12% weak decay

TABLE I: Parameters of the calculation with variances-obtained using Eq. (13,15).

$T(MeV)$	η_f	$\Delta\tau(fm/c)$	$R_{WS}(fm)$	$a_{WS}(fm)$	$w_0(fm^{-2})$	w_2	$\tau_0(fm/c)$	$\Delta\eta$	$\mu_\pi(MeV)$
214.8	1.539	2.650	12.070	0.786	0.142	$0.582 + i0.123$	8.14	1.040	122.7
± 1.6	± 0.025	± 0.07	± 0.06	± 0.015	± 0.046	$\pm 0.014 \pm 0.002$	± 0.10	± 0.032	± 1.1

TABLE II: Two Parameters Sets The first row is obtained using Eq. (13,15). The second row is obtained using Eq. (11,14). The differences with the results of Table I arise from using an improved fitting procedure.

$T(MeV)$	η_f	$\Delta\tau(fm/c)$	$R_{WS}(fm)$	$a_{WS}(fm)$	$w_0(fm^{-2})$	w_2	$\tau_0(fm/c)$	$\Delta\eta$	$\mu_\pi(MeV)$
222.1	1.639	2.660	12.049	0.717	0.113	$0.725 + i0.128$	8.14	0.997	123.9
223.5	1.593	2.687	12.166	0.819	0.161	$0.587 + i0.129$	8.198	1.01	118.5

correction of the published spectrum[22] and then multiplying by $\sqrt{\lambda(p_T)}$ as determined by a linear fit to the measured HBT values of λ . This “non-resonant pion” spectrum vs. p_T was then used to obtain a new combined description of the HBT radii and pion spectrum. After the spectrum was calculated it was “uncorrected” for comparison with the published spectrum. This calculation supplies a consistent treatment of the spectrum and radii. We therefore account for the “halo” effects of pions produced by resonances [23]. The effects of the two changes in the spectrum tend cancel each other, and their net effect on the fits is primarily an increase in temperature and flow parameters. The fit parameters are shown in Table 1. Spectral data for the low K_T region exist[24], but the value of λ are not known, so we do not include these in our current fitting procedure.

It is interesting to display our computed wave functions, and this is done in Fig. 5. The exact solutions of the wave equation differ very much from the eikonal solutions at each of the energies we consider. The maxima and minima result from the interference effects caused by the optical potential as incorporated by solving the quantum mechanical wave equation. The differences grow smaller as the value of K_T increases.

An additional point to recall is that there are at least two ways to determine the HBT radii. One is to use the quadratic form (13) for very small magnitudes of \mathbf{q} and the other is to use the Gaussian form (11) for values of \mathbf{q} that correspond to the measurements. We used the former (with $q = K_T/40$) in obtaining the results of Ref. [10]. The latter gives very similar descriptions of the data with almost the same parameters to be extracted. A comparison between the parameters obtained using the two procedures is presented in Table 2. Only minor changes are seen in the parameters. The computed radii, however, do differ significantly for values of $K_T < 175$ MeV/c. Note also that the values of the extracted temperatures are sensitive to the details of the treatment of resonances. A more accurate treatment of the K_T dependence of λ leads to about a 10% reduction in the value of the extracted temperature.

C. Non-central Au+Au

The STAR collaboration performed measurements of pionic correlations and spectra as a function of centrality. For non-central events, our optical potential would depend on the direction of \mathbf{b} as well as its magnitude. The simple dependence on b was exploited heavily in previous sections to simplify the calculations. However, we may make estimates for small deviations from perfect centrality. The nucleus-nucleus impact parameter B is related to the centrality by Glauber calculations [25], with each centrality bin of the data connected to a particular value of B . The area of the “football”-shaped overlap region formed by two circles of radius R_{WS} with centers separated by a distance B is computed and set equal to $\pi R_{WS}^2(B)$. Note that $R_{WS}(B = 0)$ is simply R_{WS} . Then $R_{WS}(B)$ is used in place of R_{WS} in the formalism described above. This amounts to taking the azimuthal average of the transverse geometry of the source, and then computing the observables. This is not the same as computing the observables for $B \neq 0$ and then taking the azimuthal averages of the observables. This is why we expect diminished accuracy for large values of B and limit these calculations to centralities of less than or equal to 20%.

The parameters R_{WS} and τ_0 are therefore reduced from the values appearing in Tables 1-2 by the ratios of the square root of the football-shaped area. We do not similarly reduce a_{WS} and $\Delta\tau$ by the same factors. Doing this would reduce the computed radii by about 5%. In the present sub-section we start with the radii obtained with the Gaussian fit to the computed correlation functions of Table 2. We do not expect that this simple geometric way of extrapolation can be accurate very far from the purely central starting point, and therefore present results for centrality of 5-10% and 10-20%. The results are shown in the Figs. 6-7. Qualitatively good

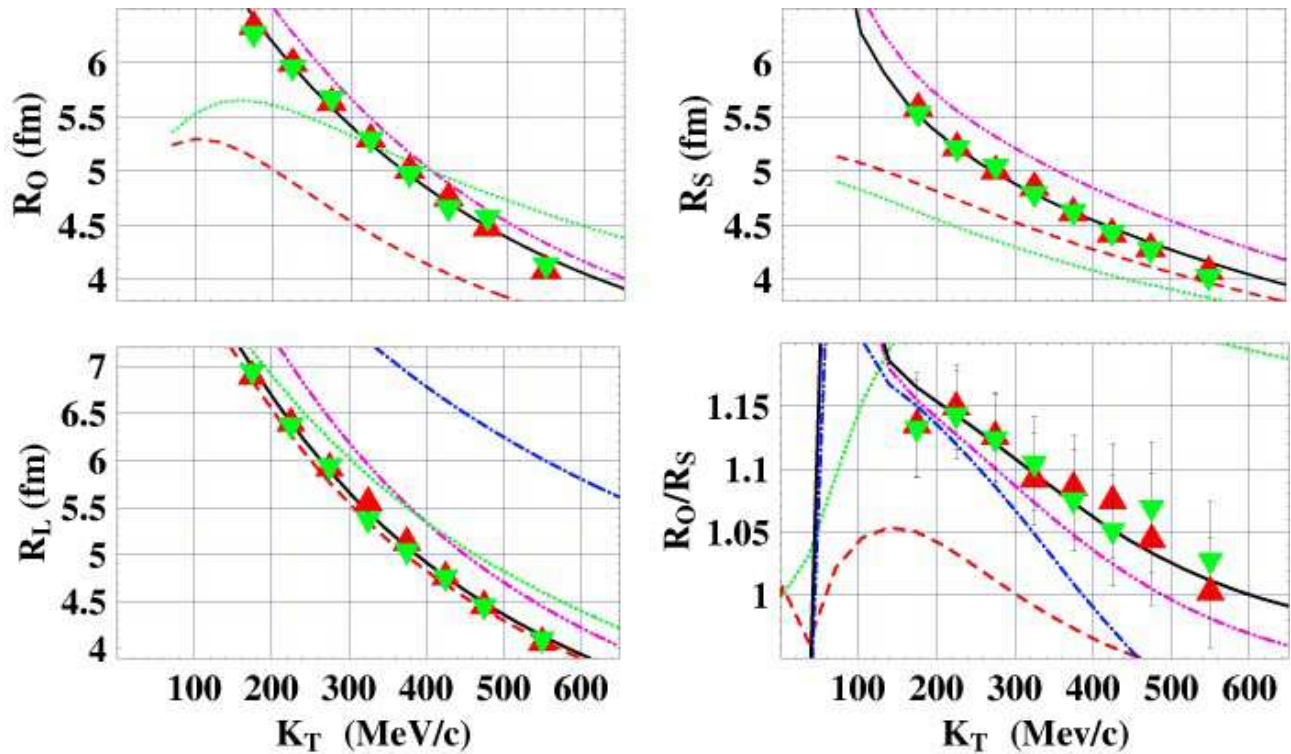


FIG. 3: (Color online) HBT Radii R_s, R_o, R_l and the ratio R_o/R_s ; Data [21]: ∇ (green) $\Rightarrow \pi^+\pi^+$; \triangle (red) $\Rightarrow \pi^-\pi^-$. Curves: solid (black) \Rightarrow full calculation; dotted (green) $\Rightarrow \eta_f = 0$ (no flow); dashed (red) $\Rightarrow \text{Re}[U]=0$ (no refraction); dot-dashed (blue) $\Rightarrow U=0$ (no potential), double-dot-dashed (magenta) \Rightarrow substituting Boltzmann for Bose-Einstein thermal distribution.

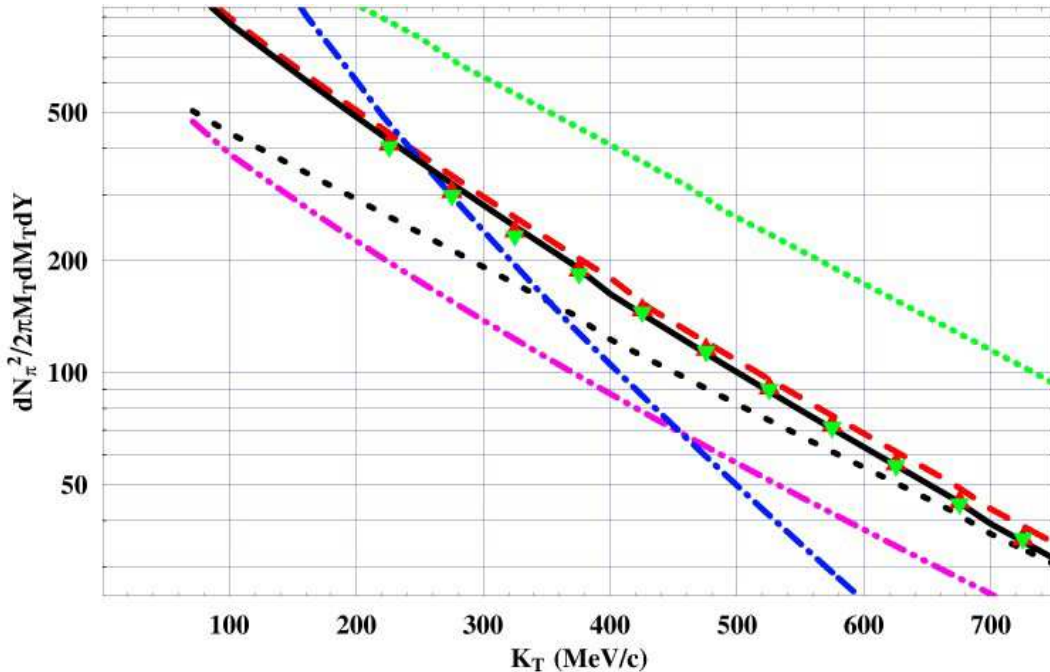


FIG. 4: (Color online) Pion momentum spectrum. Data [22]: ∇ (green) $\Rightarrow \pi^+$; \triangle (red) $\Rightarrow \pi^-$. Black dotted line is the ‘non-resonant pion’ spectrum used in the fit.

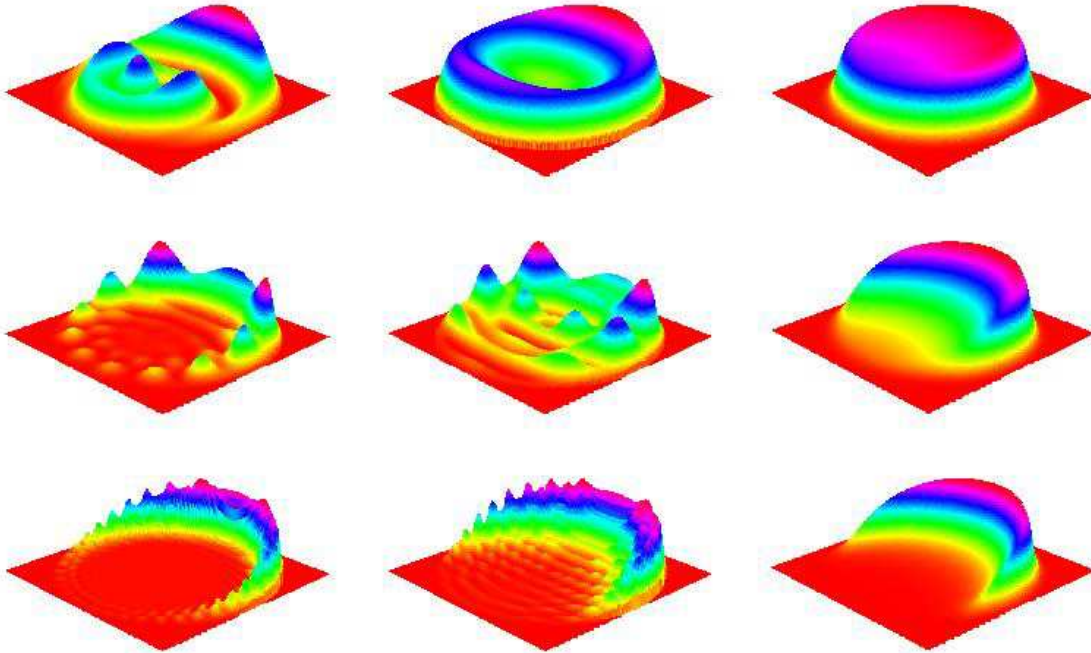


FIG. 5: (Color online) Wave functions. The figures show the absolute square of the calculated wave functions times the density $\rho(b)$. For each (row) value of K_T (.125, 1.0, 3.0 fm^{-1}), the full calculation, the calculation including only the imaginary part of the optical potential and the eikonal approximation are shown horizontally. The out direction is parallel to the lower right edge of each picture.

agreement is achieved.

D. Predictions for Cu+Cu central collisions

The STAR collaboration has also measured (but not yet published) radii and spectra for Cu+Cu collisions, so it is of interest to make predictions. This necessarily involves assumptions because our approach does not provide a complete dynamical treatment. We make the major assumption that the matter formed in the Cu+Cu collisions is of the same type as that in the Au+Au collisions. Under that assumption, the radius R_{WS} and τ_0 would be the only parameters expected to change significantly. We use a simple geometric model in which $R_{WS}, \tau_0 \propto A^{1/3}$. This give a Au/Cu ratio of 1.46 Another variation is to obtain the ratio Au to Cu parameters by using nuclear radii determined from electron scattering[26]. This gives a ratio of 1.37. Another variation is to also let a_{WS} and $\Delta\tau$ have the same A dependence as the larger parameters. In the present calculation we use Eq. (14) to obtain the radii ($q = 0.15 \text{ fm}^{-1}$). The results for radii are shown in Fig. 8 and those for spectra are shown in Fig. 9. The spread in these curves gives a reasonable expectation for the uncertainties in our predictions.

E. Exact numerical evaluation of correlation function

We present an alternate calculation al technique that gives the correlation function for any value of \mathbf{q} . To do this, start by recalling Eqs. (59) and (53) and note the appearance of the integral

$$I_{\tau\eta} \equiv \frac{1}{\sqrt{2\pi}\Delta\tau} \int_{-\infty}^{\infty} d\eta \cosh \eta \exp(-\gamma_n(b) \cosh \eta) \exp\left(-\frac{\eta^2}{2(\Delta\eta)^2}\right)$$

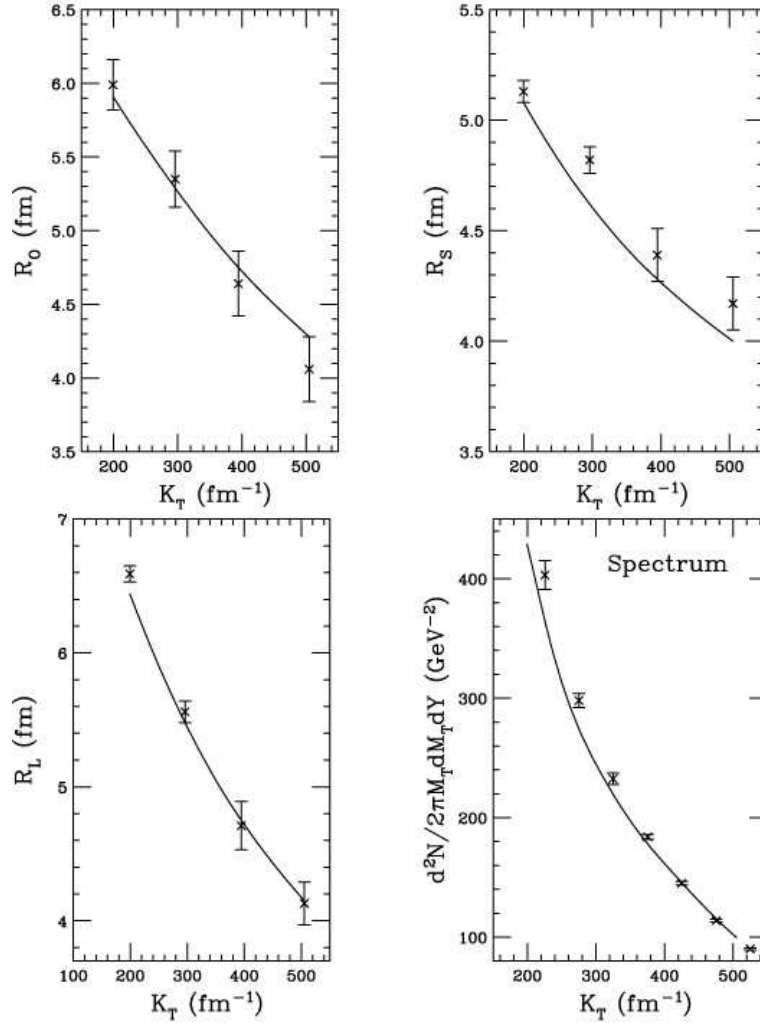


FIG. 6: Computed (not fit) values of radii R_O, R_S, R_L and pion spectrum. Obtained from the geometric scaling discussed in the text, for events of 5-10% centrality. $AuAu$ at $\sqrt{s} = 200\text{GeV}$.

$$\begin{aligned}
 & \int_{-\infty}^{\infty} \tau d\tau \exp\left(-\frac{(\tau - \tau_0)^2}{2(\Delta\tau)^2}\right) e^{i\tau((\omega_2 - \omega_1) \cosh \eta - i q_L \sinh \eta)} \\
 &= \int_{-\infty}^{\infty} d\eta \cosh \eta \exp(-\gamma_n(b) \cosh \eta + i\alpha\tau_0) \exp\left(-\frac{\eta^2}{2(\Delta\eta)^2}\right) (\tau_0 + i\alpha\Delta\tau^2) \exp(-\alpha^2\Delta\tau^2/2), \\
 & \alpha \equiv (\omega_2 - \omega_1) \cosh \eta - q_L \sinh \eta.
 \end{aligned} \tag{96}$$

The procedure of this section is to evaluate the integral over η numerically.

Let's set up the full calculation. Integrating over τ and using the result (96) yields

$$\begin{aligned}
 \int d^4x S(x, K, q) &= \sum_{n=1}^{\infty} \int d^2b B_n(\mathbf{b}, \mathbf{K}_T) \psi_{\mathbf{p}_1}^{(-)}(\mathbf{b}) \psi_{\mathbf{p}_2}^{(-)*}(\mathbf{b}) \times \\
 & \int_{-\infty}^{\infty} d\eta \cosh \eta \exp(-\gamma_n(b) \cosh \eta + i\alpha\tau_0) \exp\left(-\frac{\eta^2}{2(\Delta\eta)^2}\right) (\tau_0 + i\alpha\Delta\tau^2) \exp(-\alpha^2\Delta\tau^2/2),
 \end{aligned} \tag{98}$$

There are some remarks to be made here: there is no need to make the approximation of Eq. (147), and the present expression is actually much more compact than (67). Possible cross terms [27] involving $q_O q_L$ are

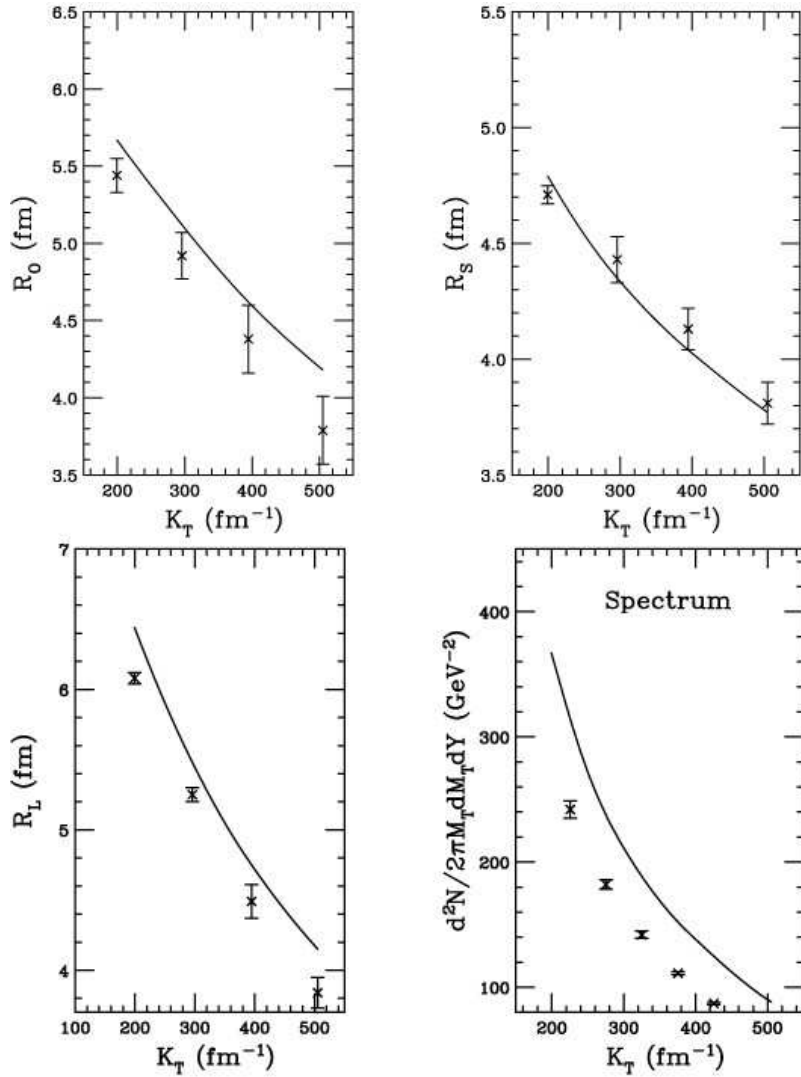


FIG. 7: Computed (not fit) radii R_O, R_S, R_L and pion spectrum. Obtained from the geometric scaling discussed in the text, for events of 10-20% centrality. $AuAu$ at $\sqrt{s} = 200$ GeV.

small for the experiments with $Y \approx 0$ that we analyze, so we neglect the cross terms and take either $q_L = 0$ or $q_O = 0$. Then the integrands have terms either even or odd in η . The odd terms cancel. So define (with $\Delta\omega \equiv \omega_2 - \omega_1$)

$$I(\gamma, \Delta\omega, q_L, \Delta\eta, \Delta\tau, \tau_0) \equiv \int_{-\infty}^{\infty} d\eta \cosh \eta \exp(-\gamma_n(b) \cosh \eta + i\alpha\tau_0) \exp\left(-\frac{\eta^2}{2(\Delta\eta)^2}\right) (\tau_0 + i\alpha\Delta\tau^2) \exp(-\alpha^2\Delta\tau^2/2). \quad (99)$$

We use various specific values of the arguments of the function I to compute the different observables. According to Eqs. (14,15) a radius R_i can be computed using $q_i \neq 0, q_{j \neq i} = 0$. Thus to compute R_O we take $q_{L,S} = 0$, so that

$$\begin{aligned} I(\gamma, \Delta\omega, 0, \Delta\eta, \Delta\tau, \tau_0) &\equiv I_O(\gamma, \Delta\omega, \Delta\eta, \Delta\tau, \tau_0) \equiv \\ &2 \int_0^{\infty} d\eta \cosh \eta \exp(-\gamma \cosh \eta) \exp\left(-\frac{\eta^2}{2(\Delta\eta)^2}\right) e^{iz\tau_0} (\tau_0 + iz\Delta\tau^2) \exp(-z^2\Delta\tau^2/2) \\ &z \equiv \Delta\omega \cosh \eta. \end{aligned} \quad (100)$$

To compute R_L we take $\Delta\omega = 0$, so that

$$I(\gamma, 0, q_L, \Delta\eta, \Delta\tau, \tau_0) \equiv I_L(\gamma, q_L, \Delta\eta, \Delta\tau, \tau_0) \equiv$$

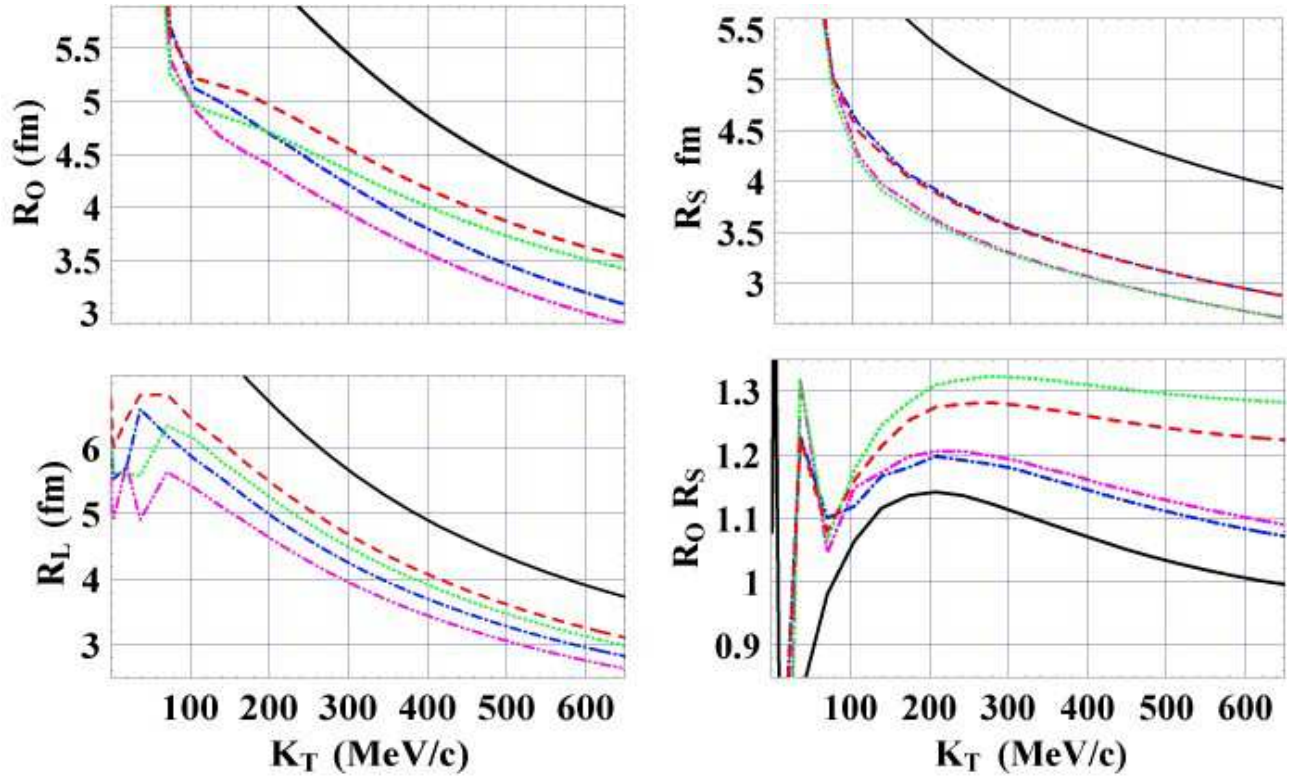


FIG. 8: (Color online) HBT Radii: Central Cu+Cu ($\sqrt{s} = 200$ GeV) predictions: long-dashed (red) - R_{WS}, τ_0 scale as the measured radii, short-dashed (green) - $R_{WS}, \tau_0, a_{WS}, \Delta\tau$ scale as the measured radii, long-dashed-dot (blue) - R_{WS}, τ_0 scale as $A^{1/3}$, long-dash-double-dotted (purple) $R_{WS}, \tau_0, a_{WS}, \Delta\tau$ scale as $A^{1/3}$; Au+Au fit - solid (black).

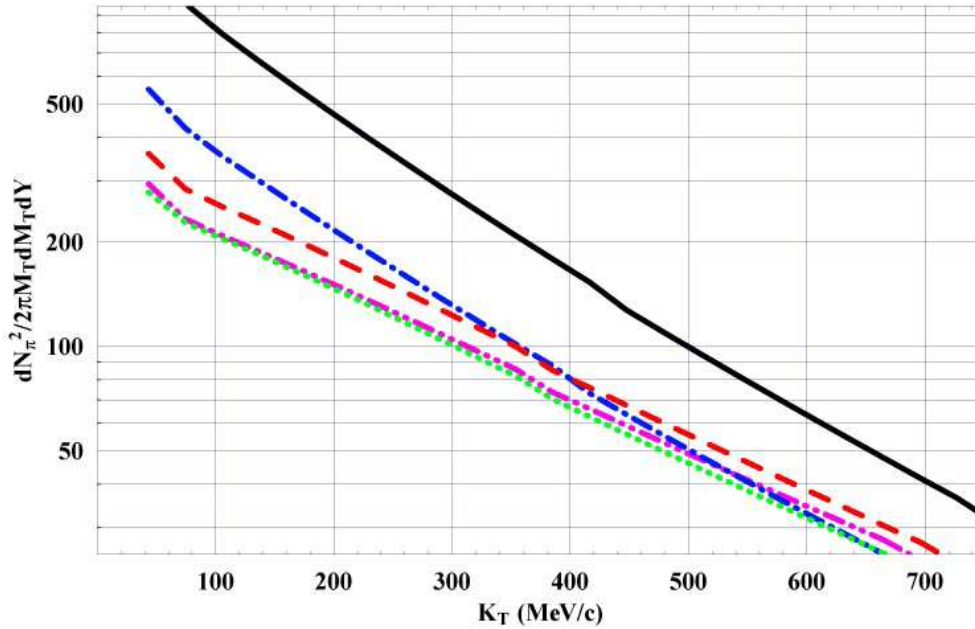


FIG. 9: (Color online) Pion Spectra: Central Cu+Cu ($\sqrt{s} = 200$ GeV) predictions: long-dashed (red) - R_{WS}, τ_0 scale as the measured radii, short-dashed (green) - $R_{WS}, \tau_0, a_{WS}, \Delta\tau$ scale as the measured radii, long-dashed-dot (blue) - R_{WS}, τ_0 scale as $A^{1/3}$, long-dash-double-dotted (purple) - $R_{WS}, \tau_0, a_{WS}, \Delta\tau$ scale as $A^{1/3}$; Au+Au fit - solid (black).

$$\begin{aligned}
& 2 \int_0^\infty d\eta \cosh \eta \exp(-\gamma \cosh \eta) \exp\left(-\frac{\eta^2}{2(\Delta\eta)^2}\right) (\tau_0 \cos(y\tau_0) - y\Delta\tau^2 \sin(y\tau_0)) \exp(-y^2\Delta\tau^2/2) \\
& y \equiv -q_L \sinh \eta
\end{aligned} \tag{101}$$

In computing R_S , the spectra, or the denominator of the correlation function we have $\Delta\omega = 0, q_L = 0$. Then we use:

$$I(\gamma, 0, 0, \Delta\eta, \Delta\tau, \tau_0) \equiv 2\tau_0 \int_0^\infty d\eta \cosh \eta \exp(-\gamma \cosh \eta) \exp\left(-\frac{\eta^2}{2(\Delta\eta)^2}\right). \tag{102}$$

Then the correlation function is given by

$$C(\mathbf{q} + q_L \hat{\mathbf{z}}, \mathbf{K}) = 1 + \frac{|\chi_{12}|^2}{\chi_{11}\chi_{22}} \tag{103}$$

$$\begin{aligned}
\chi_{12} &= \int d^4x S(x, K, q) \\
&= \sum_{n=1}^{\infty} \int d^2b B_n(\mathbf{b}, \mathbf{K}_T) I(\gamma_n(b), \Delta\omega, q_L, \Delta\eta, \Delta\tau, \tau_0) \psi_{\mathbf{p}_1}^{(-)}(\mathbf{b}) \psi_{\mathbf{p}_2}^{(-)*}(\mathbf{b})
\end{aligned} \tag{104}$$

$$\chi_{ii} = \sum_{n=1}^{\infty} \int d^2b B_n(\mathbf{b}, \mathbf{p}_i) I(\gamma_n(b), 0, 0, \Delta\eta, \Delta\tau, \tau_0) \left| \psi_{\mathbf{p}_i}^{(-)}(\mathbf{b}) \right|^2 \tag{105}$$

For very small values of \mathbf{q} this correlation function reduces to the one obtained in second order, (74). There are two changes. If \mathbf{q} is not small then get correct correlation function. A second change is that the approximation (147) is not used. The differences between using the procedure of this subsection and that of the previous subsection are negligible ($< 2\%$ and indistinguishable) for the cases we have studied. This provides a further verification of the approximations used in Sect. (VIII A), but the present formalism avoids that approximation.

F. Correlation functions and the Gaussian approximation

We apply the present formalism to obtain correlation function C (with $\lambda = 1$), using the parameters of Table I, for $K_T = 158, 316$ MeV/c. The results are shown in Figs. 10,11. We see that the correlation functions are fairly well represented by Gaussians with widths that are approximately independent of K_T . For a typical radius of about 7 fm, and $q = 0.15$ fm $^{-1}$, (where data are measured) $q^2 R^2 \approx 1$ so using the approximation (13) is not very accurate. Nevertheless, the correlation functions are close to Gaussian in shape. A more detailed look at the ratio of computed correlation functions ($C - 1$) to its Gaussian fit in Fig. 11 shows that the Gaussian curves represent the correlation functions fairly well in the region $0 < q < 0.22$ fm $^{-1}$ where $C - 1$ is large, but are larger (for $R_{O,L}$) or smaller (for R_S) than the Gaussian fit for $q > 0.22$ fm in the “tail” region.

G. Possible Extensions of the DWEF Model

The DWEF model presented here uses the empirical “hydrodynamics-inspired” emission function of Eq. (26). However, we note that the application of distorted waves to an emission function is more generally applicable, and that the formalism we present here can be applied to any emission function that has the same symmetry properties as Eq. (26). One extension of the model would be to calculate the emission function as a multi-dimensional numerical table directly from hydrodynamics and use this with the DWEF model to calculate spectra and radii. We also note that, while it has not been implemented here, the DWEF model allows the temperature and chemical potential to depend on b , as is done in the Buda-Lund model [20].

IX. THE EIKONAL APPROXIMATION

Several previous calculations [28]–[31] of the effects of opacity have used the eikonal approximation to solving the wave equation (39). Here we explain the nature of this approximation and discuss its weaknesses and (fewer) strengths when applied to the current situation.

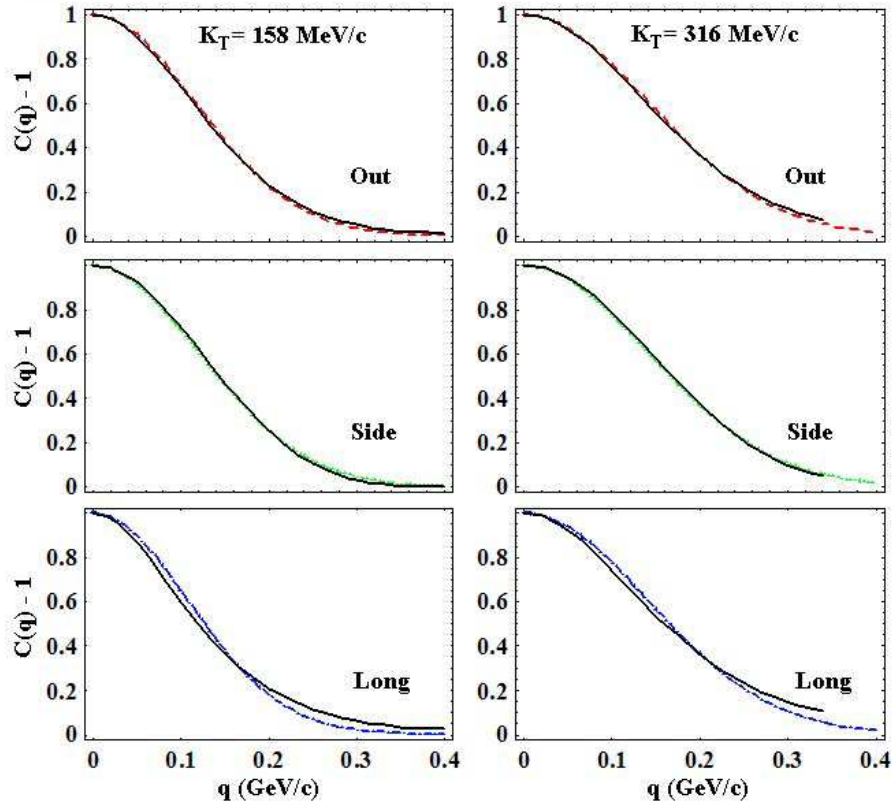


FIG. 10: (ColorOnline) Central $AuAu$ ($\sqrt{s}=200$ GeV). Correlation functions ($K_T=158$, 316 MeV/c) for the out, side and longitudinal cases. The solid (black) curves are the full correlation functions. The broken curves are Gaussian fits: dash for out, dot for side and dot-dash for longitudinal.

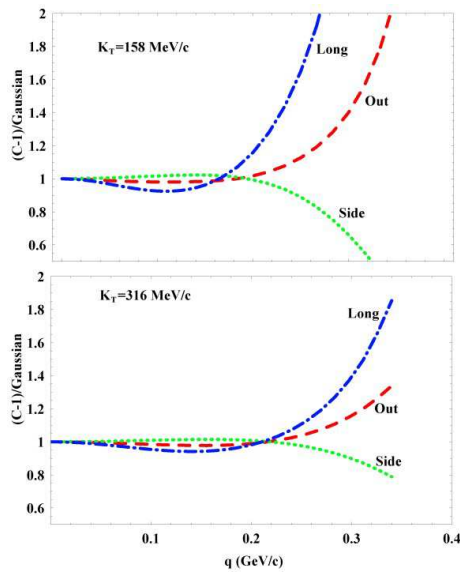


FIG. 11: (Color Online) Central $AuAu$ ($\sqrt{s}=200$ GeV). Ratios of correlation functions ($K_T=158$, 316 MeV/c) to Gaussian fits for the out, side and longitudinal cases. The dashed (red) curves are obtained with \mathbf{q} in the out direction, the dotted (green) curves with \mathbf{q} in the side direction, and the dot-dashed (blue) curves with \mathbf{q} in the longitudinal direction.

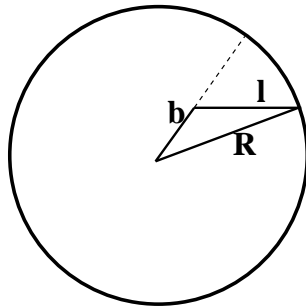


FIG. 12: Eikonal calculation of pion wave function. A pion produced at a position \mathbf{b} propagates along a straight line path \mathbf{l} until it hits the edge of the medium, denoted by \mathbf{R} . The angle between the dashed line and the horizontal line \mathbf{l} is denoted in the text as θ_s . The out case with $\theta_s = 0$ is shown.

The basic idea is that if the momentum is large one may say approximately that the wave propagate in a given direction (here the out direction, which is taken as along the x axis). Then one assumes a solution of the form $\psi^{(-)*}(\mathbf{b}) = e^{ipx}\Phi(\mathbf{b})$ that is inserted into the wave equation. Taking the Laplacian of the approximate wave function gives a term proportional to p^2 that is canceled, a term proportional to p that is kept, and another term that is ignored. Then one finds

$$\psi^{(-)*}(\mathbf{b} = x, y) = e^{ipx} \exp \left[\frac{-i}{2p} \int_x^\infty U(x', y) dx' \right]. \quad (106)$$

for propagation in the x (out) direction. The corrections to this solution are of order $\frac{-1}{2iK} \frac{1}{U} \frac{\partial U}{\partial x} - \frac{U}{4K^2}$ times the terms that are kept. The first correction can be large in the surface region in which U varies greatly and the second term can be large in the interior region in which U reaches its full value. We are concerned with pions of momentum ranging from 30 to 600 MeV/c, so that the eikonal approximation be expected to be poor. However the ease of application, and its wide use makes it worthwhile for us to assess the use of Eq. (106). We consider a purely imaginary potential first and then use a general complex potential.

A. Strong Absorption at High K – Purely Imaginary potential

In the impulse approximation $U = -4\pi f\rho$ where f is the projectile-target scattering amplitude and ρ is the density of scatterers. The optical theorem relates the imaginary part of f to the total cross section σ so that $Im[U] = -p\sigma\rho$. If we keep only the imaginary potential $-i/(2p)U = 1/2\sigma\rho$ and for a constant density the intensity of the wave falls as $e^{-x\lambda_{\text{mfp}}}$ with the mean free path, $\lambda_{\text{mfp}} = \frac{1}{\sigma\rho}$. More generally the wave function for a purely imaginary optical potential is given by

$$\psi^{(-)}(\mathbf{p}_i, \mathbf{b}) = e^{-i\mathbf{p}_i \cdot \mathbf{b}} e^{-l_i/2\lambda_{\text{mfp}}} \quad (107)$$

where $i = 1, 2$ for the two wave functions and $l_i(\mathbf{b}, \mathbf{K})$ is the direct line path length (parallel to the direction of \mathbf{p}_i from the emission point \mathbf{b} to the edge of the medium. For a purely imaginary optical potential $U = -iK\sigma\rho$ and λ_{mfp} is the resulting mean free path.

We have, see Fig. 12

$$\mathbf{R} = \mathbf{l}_i + \mathbf{b}, \quad (108)$$

$$R^2 = l_i^2 + b^2 + 2bl_i \cos(\theta - \theta_s). \quad (109)$$

θ is angle between \mathbf{b} and x -axis (direction of \mathbf{K}) θ_s is angle between $\mathbf{p}_{1,2}$ and \mathbf{K} . This was called α in previous sections. The angle between \mathbf{b} and \mathbf{l}_i is $\theta - \theta_s$. Solving we find

$$l = -b \cos(\theta - \theta_s) + \sqrt{(b \cos(\theta - \theta_s))^2 + R^2 - b^2}. \quad (110)$$

For the R-out case $\theta_s = 0$, and

$$l_i = l = -x + \sqrt{R^2 - y^2} \quad (111)$$

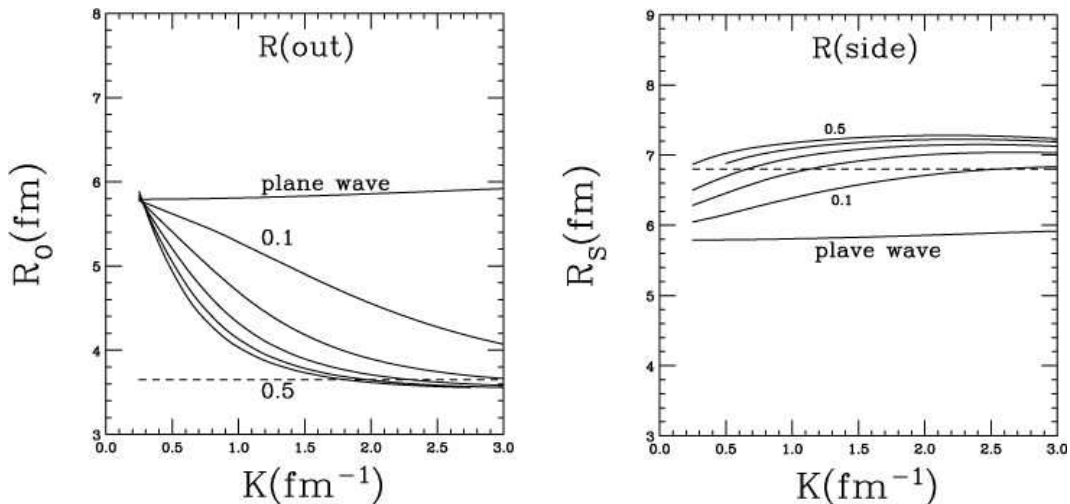


FIG. 13: Radii R_o and R_s for increasing values of $Im[w_2]$. All other optical potential parameters and the flow parameters are set to 0. The numbers in the figure refer to the range of values. The dashed curve shows the result of Heiselberg & Vischer.

In this approximation the correlation function minus one is given by the absolute square of the ratio of integrals: $\frac{I_{\parallel,\perp}(q)}{I_{\parallel,\perp}(q=0)}$. In particular,

$$I_{\parallel}(q) = \int d^2b e^{i\mathbf{q}\cdot\mathbf{b}} e^{-l/\lambda_{\text{mfp}}}, \quad \mathbf{q} \parallel \hat{\mathbf{x}} \quad (112)$$

$$= \frac{\lambda}{1+iq\lambda} \int_{-R}^R dy \left(e^{iq\sqrt{R^2-y^2}} - e^{-(iq+2/\lambda_{\text{mfp}})\sqrt{R^2-y^2}} \right). \quad (113)$$

If $\lambda_{\text{mfp}} \ll R$ we neglect the second term. Since we are interested in radii, we expand the remaining term in powers of the exponential (keeping $\lambda_{\text{mfp}} \ll R$):

$$I_{\parallel}(q) = \frac{\lambda_{\text{mfp}}}{1+iq\lambda_{\text{mfp}}} (2R - q^2 R^2/2(2R - 2R/3) + iq\pi R/2) \quad (114)$$

$$C_{\parallel}(q) \approx 2 - q^2 R^2(2/3 - \pi^2/16) \quad (115)$$

$$R_O^2 = R^2(2/3 - \pi^2/16) = 0.0498R^2; R_O = R/4.48 \quad (116)$$

In the plane wave approximation (Eq. (113) with $\lambda_{\text{mfp}} \rightarrow \infty$) one would find $R_O^{PW} = R/\sqrt{8}$. The striking result of Heiselberg & Vischer[28] indicated that the measured radius should be 40% smaller than the radius obtained in plane wave approximation. This result is confirmed for the highest value of $K_T = 3 \text{ fm}^{-1} \approx 600 \text{ MeV}/c$ by the calculations shown above in Fig. 2. The value of R_o is reduced by approximately 40% by the influence of the imaginary optical potential. Fig. 13 shows the effects of increasing the imaginary potential (by varying $Im[w_2]$ from 0.1 to 0.5 in steps of 0.1). The computed value of R_O does not change when $Im[w_2]$ is large enough and K_T is high enough. Small deviations between our results for highest K_T and the result[28] can be attributed to the non-zero value of the diffuseness a_{WS} .

In the model of the present section, the correlation function and pion intensity would each be proportional to λ_{mfp} , and a very small value would yield a very small pionic spectrum. More generally, the extraction of the chemical potential from the pionic spectrum depends on the mean free path parameter λ_{mfp} .

Now let us do the R-side case. Then

$$\cos \theta_s = \frac{K}{\sqrt{K^2 + q^2/4}}; \sin \theta_s = \pm \frac{q/2}{\sqrt{K^2 + q^2/4}} \quad (117)$$

$$\cos(\theta - \theta_s) = \cos \theta \left(1 - \frac{q^2}{8K^2}\right) \mp \frac{q}{2K} \sin \theta. \quad (118)$$

We find that

$$l_i \rightarrow -x + \sqrt{R^2 - y^2} \pm \mathcal{O}\left(\frac{q}{K}\right) + \mathcal{O}\left(\frac{q^2}{K^2}\right) \approx -x + \sqrt{R^2 - y^2}. \quad (119)$$

The terms $\pm\mathcal{O}(\frac{q}{K})$ cancel in computing the term l_1+l_2 that enters in computing the present correlation function. Thus the correction is of order $1/K^2$. The eikonal approximation works only if $KR \gg 1$, so the corrections must be presumed to be small. Then

$$I_{\perp}(q) = \int_{-R}^R dy e^{iqy} \int_{-\sqrt{R^2-y^2}}^{\sqrt{R^2-y^2}} dx e^{x/\lambda_{\text{mfp}}} e^{-\frac{1}{\lambda_{\text{mfp}}}\sqrt{R^2-y^2}} \quad (120)$$

$$\approx \lambda \int_{-R}^R dy (1 - q^2 y^2 / 2) = \lambda_{\text{mfp}} (2R - q^2 R^3 / 3) \quad (121)$$

$$C_{\perp}(q) = 2 - q^2 R^2 / 3 \quad (122)$$

$$R_s^2 = R^2 / 3, \quad (123)$$

Without distortion would be $C_{\perp}^{PW}(q) = 2 - q^2 R^2 / 4$, so in this case the strong absorption increases the radius by a factor of $\sqrt{4/3}$. This result is qualitatively obeyed in our realistic solutions of the wave equation, see Fig. 13.

B. Complex potential with non-vanishing real part

If there is an attractive real potential the wave function of Eq.(107) becomes:

$$\psi^{(-)}(\mathbf{p}_1, \mathbf{b}) = e^{-i\mathbf{p}_1 \cdot \mathbf{b}} e^{-l_1(1+i\alpha)/2\lambda_{\text{mfp}}} \quad (124)$$

with α dimensionless, real and positive. If $\alpha = 0$ one obtains the purely absorptive model of the previous sub-section. Conversely, the limit of a purely real potential occurs when $1/\lambda_{\text{mfp}} \rightarrow 0, \alpha/\lambda_{\text{mfp}} \rightarrow 1/\lambda_0$. We also have

$$\psi^{*(-)}(\mathbf{p}_2, \mathbf{b}) = e^{i\mathbf{p}_2 \cdot \mathbf{b}} e^{-l_2(1-i\alpha)/2\lambda_{\text{mfp}}} \quad (125)$$

In the product $\psi_{\mathbf{p}_1} \psi_{\mathbf{p}_2}^*$ enters in computing the correlation function, so unlike the previous case of pure absorption, a term of the form $l_1 - l_2$ enters. This difference is of order q/K compared to other terms, but its influence in computing radii must lead eventually to a term of order $(\frac{q}{K})^2$. The validity of the eikonal approximation depends on the ability to disregard such terms. Thus a valid eikonal approximation means that $l_1 = l_2$ so the factors of α cancel out in the product $\psi^{(-)}(\mathbf{p}_1, \mathbf{b}) \psi^{*(-)}(\mathbf{p}_2, \mathbf{b})$. Thus, if one assumes the eikonal approximation is valid at all values of K_T , one would find erroneously that the real potential never has an influence on the calculation of HBT radii.

Unlike the effects of the imaginary potential, which are qualitatively captured by the eikonal approximation (even if applied wrongly at low values of K_T), the effects of the real potential are completely lost. Thus the eikonal approximation can not be used for values of K_T such that the real potential contributes. As shown in Fig. 3 the real potential is important for all values of K_T less than 600 MeV/c. Conversely, for much larger values of K_T , for which the eikonal approximation does accurately reproduce the solution of the wave equation, the real potential will not play a role in determining radii.

X. CHIRAL SYMMETRY RESTORATION

As discussed above, our approach to obtaining the optical potential U is phenomenological—we use Eq. (95). This assumes nothing about the nature of the dense medium. Some simple ideas regarding the expected size of U are presented in Sec.V. In the present section, we investigate the influence of chiral symmetry and its possible restoration.

Suppose the dense medium is one in which chiral symmetry is restored. This means that the value of the quark condensate vanishes, an effect that could be caused by an increase in temperature or density. The pion mass is proportional to the quark condensate via the GMOR relation

$$m_{\pi}^2 f_{\pi}^2 = -\frac{m_u + m_d}{2} \langle 0 | \bar{u}u + \bar{d}d | 0 \rangle, \quad (126)$$

where f_{π} is the weak pion decay constant ≈ 93 MeV. It is believed that m_{π}, f_{π} and the condensate $\langle 0 | \bar{u}u + \bar{d}d | 0 \rangle$ all depend on temperature and density. If one takes the Brown-Rho[32] scaling relation for f_{π} and the perturbative

calculated temperature dependence of the condensate, the pion mass is proportional to the cube root of the condensate, and therefore vanishes for sufficiently large temperatures. See the reviews [33]. Suppose the optical potential arises *only* from the temperature dependence of the pion mass. Then the two-dimensional Klein-Gordon equation would take the form:

$$(-\nabla^2 + m_\pi^2(T))\psi = (p^2 + m_\pi^2)\psi, \quad (127)$$

for regions inside the medium. Our wave equation is shown as Eq. (39). Comparing Eq. (127) with Eq. (39) shows that one obtains the optical potential

$$U(b) = (m_\pi^2(T) - m_\pi^2)\rho(b), \quad (128)$$

in which the finite extent of the medium is accounted for by the factor $\rho(b)$. This amounts to having a real potential that is independent of momentum. In this case, the imaginary potential should be proportional to the momentum of the pion.

A more recent study by Son & Stephenov[34] accounts for chiral symmetry by including the general p -wave nature of the low-energy interaction between pions and any target. These authors employ the dispersion relation for low momentum pions in infinite nuclear matter[34, 35]:

$$\omega^2 = u_\pi^2(\hat{p}^2 + m_\pi(T)^2), \quad (129)$$

where \hat{p}^2 is the infinite-sized matter version of $-\nabla^2$. The quantity u_π is termed the pion velocity, even though it is only that when $m_\pi(T)$ vanishes. The term $m_\pi(T)$ is denoted the pion screening mass. This quantity appears in the expression for the static Euclidean pion correlator[34]. The energy of a pion at $\mathbf{p} = 0$ is termed the pion pole mass. The free pion mass is m_π . In Ref. [34] Eq. (129) applies only for $T < T_c$. For larger temperatures, chiral symmetry is restored and pions are massless.

Defining $t \equiv (T_c - T)/T_c$, SS find $m_\pi^2(T) \sim t^{\beta-\nu}$, $u^2 \sim t^\beta$, with $\beta < \nu$, e.g $\nu = .73, \beta = .38$ [36]. These equations are valid for temperature close to (but not too close to) the critical point. Another view about the dispersion relation can be found in Ref. [37]. This general discussion about the influence of chiral resotration provides some guidance, but does not tell us exactly to use.

We wish to obtain an equivalent optical potential and see if it is attractive or repulsive. Use the Klein Gordon equation in the form

$$\hat{p}^2 + U + m_\pi^2 = p^2 + m_\pi^2. \quad (130)$$

The term $\omega^2 = p^2 + m_\pi^2$ to obtain the correct wave equation in regions outside the dense medium where $U = 0$. Subtract (130) from (129) to obtain

$$U = u_\pi^2 m_\pi^2(T) - m_\pi^2 + (u_\pi^2 - 1)\hat{p}^2, \quad (131)$$

an expression that is the sum of two negative definite terms. This form can be simplified by using the wave equation (130) to remove term \hat{p}^2 . Then one finds a momentum-dependent optical potential:

$$U = \frac{u_\pi^2 m_\pi^2(T) - m_\pi^2 + (u_\pi^2 - 1)p^2}{u_\pi^2} \quad (132)$$

of the general form of Eq. (95) (for regions where $\rho(b)$ is constant). Note that if u_π becomes really small the optical potential becomes very strongly attractive.

For matter of finite size, the term \hat{p}^2 can also be interpreted as $-\nabla \cdot c \nabla$. For infinite nuclear matter only forward scattering occurs and the two terms are identical, but differences may arise for scattering from media of finite size. One can not tell the difference between the two terms at the start, so that we find a general form

$$U_p(b) = (a + bp^2)\rho(b) - c\nabla\rho(b) \cdot \nabla, \quad (133)$$

with both the real and imaginary parts of a, b, c negative for attractive interactions. This simple form is strictly valid only for low-energy pions. We use Eq. (95) in our present numerical calculations. For media of sufficiently large size, using the gradient term should not affect the results much, and our numerical results are consistent with this expectation.

XI. OSCILLATIONS – A SIMPLE SQUARE WELL EXAMPLE

Our numerical results are that the radii may have significant oscillations for small values of $K_T = K$. The purpose of this sub-section is to provide a simple example that also yields oscillating radii. Consider a cylindrical source of radius R of infinite extent in the longitudinal direction. Suppose this leads to a real, attractive square well potential of radius R that is proportional to the square of the momentum, as motivated by Eq. (95). Then (39) becomes

$$(-\nabla^2 - U_0 p^2)\psi = p^2\psi \quad (b \leq R) \quad (134)$$

$$-\nabla^2\psi = p^2\psi \quad (b > R), \quad (135)$$

with $U_0 > 0$. This equation is easily solved using the partial wave expansion (43). To provide a simple analytic example we further specify to the case of the lowest partial wave, $m = 0$. In this case we find

$$\psi(\mathbf{b}) = J_0(p\sqrt{1+U_0}b), \quad (b \leq R) \quad (136)$$

This shows immediately that the effect of the interaction is to scale each momenta p_1, p_2, K by a factor $\sqrt{1+U_0}$. We define

$$\tilde{p} \equiv p\sqrt{1+U_0}. \quad (137)$$

Eq. (136) is a valid approximation to the full wave function (for $b \leq R$) only if $p(\sqrt{1+U_0}R) \ll 1$. However, it is interesting to also consider larger values of p .

To compute radii, recall the correlation function (59). For simplicity we take $\eta_f = 0$, and consider fixed values of η and τ , with $\Delta\tau = 0$. This corresponds to evaluating S_0 at its peak and neglecting the influence of time duration. In this case many factors in the numerator and denominator of Eq. (60) cancel. Then the correlation function is given by a simple expression that provides some insight:

$$C(K, q) - 1 = \frac{\phi_R^2(\tilde{p}_1, \tilde{p}_2)}{\phi_R(\tilde{p}_1)\phi_R(\tilde{p}_2)} \quad (138)$$

$$\phi_R(p_i, p_j) \equiv \frac{1}{R^2} \int_0^R b db J_0(p_i b) J_0(p_j b) = \frac{p_i J_0(p_j R) J_1(p_i R) - p_j J_0(p_i R) J_1(p_j R)}{R(p_i^2 - p_j^2)} \quad (139)$$

$$\phi_R(p_i) \equiv \frac{1}{R^2} \int_0^R b db J_0^2(p_i b) = \frac{1}{2} (J_0^2(p_i R) + J_1^2(p_i R)) \quad (140)$$

If we are concerned with the side radius, inside the well $p_1 = p_2 = \sqrt{K^2 + q^2/4}$ for the three arguments, K, p_1, p_2 of J_0 that enter. Then the radius vanishes. This is a specific consequence of the approximation of taking only $m = 0$ —all directions of \mathbf{K} are equivalent, so there is no influence of vectors \mathbf{q} that are perpendicular to \mathbf{K} .

The out case is more interesting because the energies and magnitudes of momenta $p_{1,2} = (K \pm q/2)$ of the two pions are different. A non-zero radius is obtained by evaluating $C(K, q)$ for very small values of q and using Eq. (15). The quantity $R_O(K)/R$ is displayed in Fig. 14. We see that the oscillatory pattern characteristic of our realistic results, such as Fig. 3 for small values of K_T emerges from the present calculation.

Another quantity of interest is the ratio of radii computed with $R_O(K)$ and without $R_O^0(K)$ the influence of distortions:

$$\frac{R_O(K)}{R_O^0(K)} \equiv \text{Ratio} \quad (141)$$

displayed in Fig. 14. The oscillations seen in the right part of Fig. 14 demonstrate the significance of final state interactions that cause enhancements by factors of greater than six and suppressions by factors of 2! Furthermore, comparing the left and right hand sides of the figure shows the quantity $R_O^0(K)/R$ also oscillates. This is caused by the sharp edge of the square well.

XII. THE SMOOTHNESS APPROXIMATION

A common approximation called the “smoothness approximation” [2], is to simplify the correlation function (24) using the replacement

$$S(x, p_1)S(y, p_2) \rightarrow S(x, K)S(y, K) \quad (142)$$

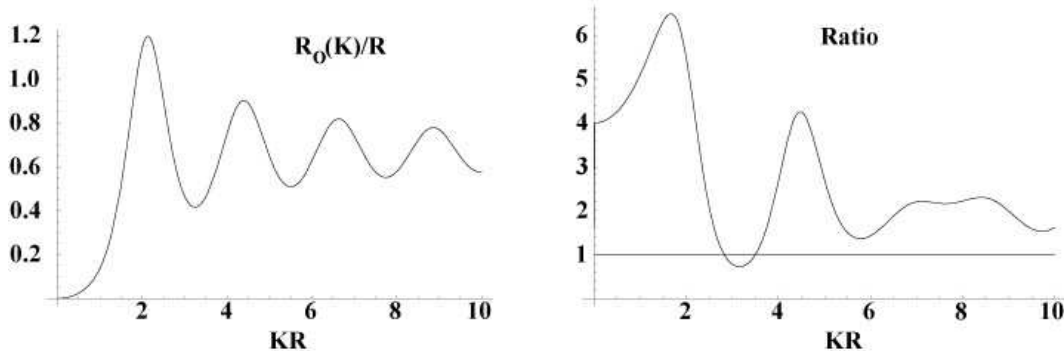


FIG. 14: $R_O(K)/R$ and the ratio of eq (141). The parameter $U_0 = 1$.

in the denominator. In this case the radii can be expressed in terms of moments of the correlation function. We note that unless the experiment has extremely good momentum resolution, the difference between the right and left hand sides of Eq. (142) will be negligible. However, for very small values of K the value of q at which the correlation function is measured may not be small compared to K and relatively large differences may occur. As noted above, there is also some ambiguity in defining K^0 because $K^\mu K_\mu \neq m_\pi^2$. Here we take $K^0 = \sqrt{\mathbf{K}^2 + m_\pi^2}$ to evaluate the spectral functions that appear in the denominator of the correlation function.

A. Simple Square well example

The example of the previous subsection can be applied to test the smoothness approximation. In the context of that example the smoothness approximation to Eq. (138) is obtained by replacing the factors $\phi_R(\tilde{p}_1)\Phi_R(\tilde{p}_j)$ by $\Phi_R(\tilde{K})^2$ appearing in the denominator of Eq. (138). Then one obtains a “smoothed” version of the radius:

$$R_O^2(K, \text{smooth}) = -2B(K)R^2/\Phi_R(K, K), \quad (143)$$

$$B(K) = \frac{-2\tilde{K}^2 J_0(\tilde{K})^2 + J_1(\tilde{K})((8 - 4\tilde{K}^2)J_1(\tilde{K}) - 3\tilde{K}J_2(\tilde{K})) + \tilde{K}J_0(\tilde{K})(-3J_1(\tilde{K}) + 2\tilde{K}J_2(\tilde{K}))}{48\tilde{K}^2}. \quad (144)$$

The low K limit is especially interesting

$$\lim_{K \rightarrow 0} R_O(K, \text{smooth}) = \frac{R}{4} \quad (145)$$

This deviation from 0 (the value of R_S vanishes) shows that the smoothness approximation violates a fundamental symmetry that the out and side radii must be the same at $K = 0$. The practical importance of this is diminished by the fact that this result emerges by first taking $q \rightarrow 0$ and then taking $K \rightarrow 0$. In real experiments q may be a fixed fraction of K as it approaches 0. Using this limit would give a vanishing value of $R_O(K \rightarrow 0)$.

The smooth version of the radius is shown in Fig. 15. The wiggles that are characteristic of the exact toy model result are greatly diminished. Indeed the strong enhancements caused by final state interactions are also greatly diminished as displayed in Fig. 15. Thus any attempts to observe oscillations require excellent momentum resolution and avoiding the smoothness approximation.

The smoothness approximation (142) violates the constraints of rotational invariance at $K = 0$. It also misses the dramatic influence of final state interactions that is the correct characteristic of this particular example. We conclude that the smoothness approximation should not be used for pions of very low momentum.

B. Realistic calculation

We can make a numerical study of the smoothness approximation using our complete calculation of Sect. VIII. The smoothness approximation is easily described within the formalism of Sect. VIII A. One merely replaces the terms Φ_{11}, Φ_{22} in Eq. (74) by the term $F_0(K_T)$ of Eq. (72). The numerical results find that the

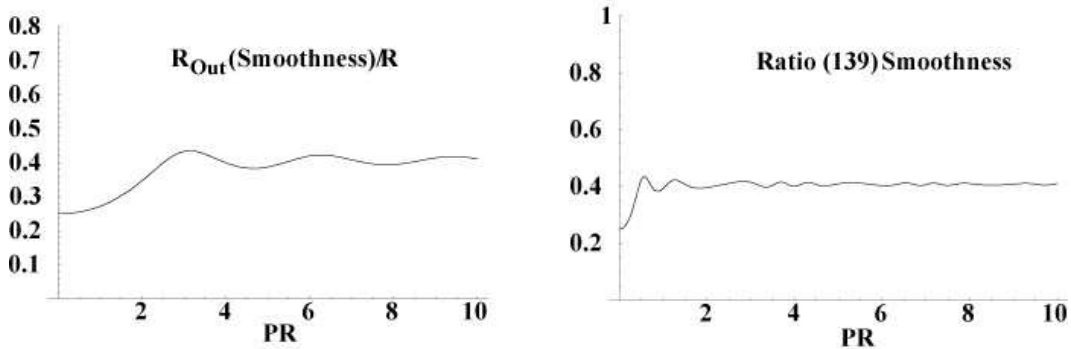


FIG. 15: Smoothness version of R_O , Eq. (145) and the ratio Eq. (141). The parameter $\alpha = 1$.

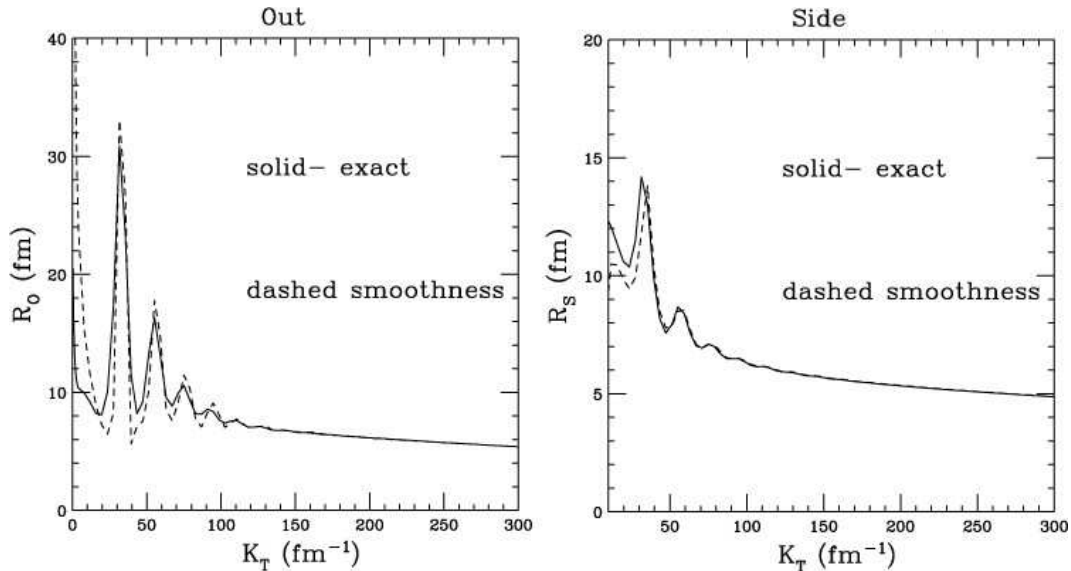


FIG. 16: Real calculation, Table 1, R_O and R_S smoothness versus exact

smoothness approximation is not good for low values of $K_T < 100$ MeV/c, but very accurate for $K_T > 160$ MeV/c. See Fig. 16.

XIII. SUMMARY

A complete formal treatment of the distorted waves treatment of HBT correlations is presented here. The need for incorporating the influence of an optical potential U and the resulting distorted wave emission function is explained. The partial wave formalism necessary to compute the pionic distorted waves and the resulting emission function is detailed. Two different methods with equivalent results to evaluate the necessary eight-dimensional integral are described. Chiral symmetry restricts the form of U [34, 35] at low energy and the necessary constraints are implemented here and in [10]. An excellent description of the STAR Au+Au HBT and spectrum data is achieved for central collisions and the use of an average area formulation leads to a very good description of these observables for non-central collisions. We also use four different versions of geometrical scaling to predict the results of central Cu+Cu collisions. The ability to calculate the absolute magnitude of the spectrum as well as the radii Eq. (14), Eq. (15) (which involve ratios of functions of emission functions) required for the computation of radii is a principal advantage of our method. The Blast Wave Model is discussed in Sec. IV.

We find that the necessary real optical potential is so strongly attractive that the pion can be said to lose its mass inside the medium. That chiral symmetry seems to be restored is the conclusion of our earlier work[10]. The RHIC-HBT puzzle is therefore replaced by the need to investigate this restoration.

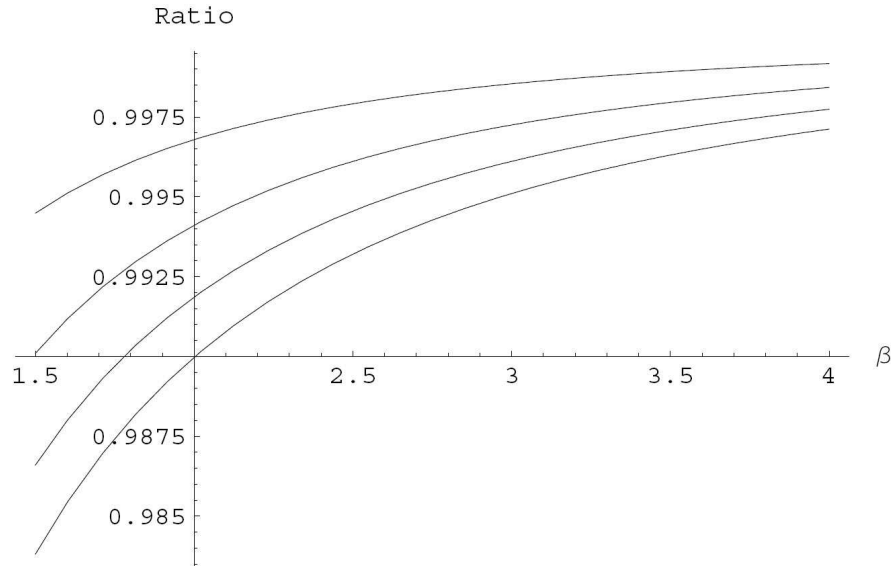


FIG. 17: The ratio of the approximate expression Eq. (147) to the exact one of Eq. (146). The values of γ range from .05 to 0.2, with ratio approaching unity as γ approaches 0.

Explicit evaluation of wave functions obtained by exact numerical solutions of the wave equation show some interesting features of the strong interaction and also display differences with the solutions obtained using the eikonal approximation. A critical discussion of the eikonal approximation as applied to computing HBT radii shows that its use causes the crucial influence of the real part of the optical potential to be entirely lost. The huge importance of the real part of the optical potential is explicitly illustrated through a simple

A final technical issue is the validity of the commonly used smoothness approximation. The approximation is shown to be very bad for low energy pions, but is very accurate if the average pion momentum is greater than about 180 MeV/c.

There are many immediate applications of this formalism. In particular, a treatment of HBT data obtained at all energies is in progress and will be presented elsewhere.

Acknowledgments

This work is partially supported by the USDOE grants Nos. DE-FG-02-97ER41014 and DE-FG-02-97ER41020. GAM thanks LBL, TJNAF and BNL for their hospitality during the course of this work. We thank W. Busza, T. Csörgő, J. Draper, M. Lisa, S. Pratt, J. Rafelski, S. Reddy and D. Son for useful discussions.

Appendix

Consider the integral appearing in Sect. VIII A:

$$f(\beta, \Delta\eta) = \int_{-\infty}^{\infty} d\eta \exp(-\eta^2/(2\Delta\eta^2)) \cosh(\eta) \exp(-\beta \cosh \eta), \quad (146)$$

that can be approximated [18] using Eq. (63) as

$$f(\beta, \Delta\eta) = 2 \exp(2\gamma) K_1(\beta + 2\gamma). \quad (147)$$

$$\gamma \equiv \frac{1}{2\Delta\eta^2}. \quad (148)$$

Figure 17 shows the approximation is excellent.

-
- [1] S. Pratt, “Two Particle And Multiparticle Measurements For The Quark - Gluon Plasma,” in Hwa, R.C. (ed.): Quark-gluon plasma, vol.2, page 700-748, 1995.
- [2] U. A. Wiedemann and U. W. Heinz, Phys. Rept. **319**, 145 (1999).
- [3] P. F. Kolb and U. Heinz, *Quark Gluon Plasma 3*, edited by R.C. Hwa and X.-N. Wang, World Scientific, Singapore, 2004)
- [4] M. Lisa, S. Pratt, R. Soltz and U. Wiedemann, arXiv:nucl-ex/0505014.
- [5] S. Pratt, Phys. Rev. Lett. **53**, 1219 (1984). G. F. Bertsch *et al.*, Phys. Rev. **C37**, 1896 (1988).
- [6] D. H. Rischke and M. Gyulassy, Nucl. Phys. A **608**, 479 (1996)
- [7] C. Adler *et al.* [STAR Collaboration], Phys. Rev. Lett. **87**, 082301 (2001); K. Adcox *et al.* [PHENIX Collaboration], Phys. Rev. Lett. **88**, 192302 (2002); A. Enokizono [PHENIX Collaboration], Nucl. Phys. A **715**, 595 (2003).
- [8] U. W. Heinz and P. F. Kolb, hep-ph/0204061.
- [9] M. Gyulassy and L. McLerran, Nucl. Phys. A **750**, 30 (2005).
- [10] J. G. Cramer, G. A. Miller, J. M. S. Wu and J. H. S. Yoon, Phys. Rev. Lett. **94**, 102302 (2005). Plus erratum.
- [11] M. Gyulassy, S. K. Kauffmann and L. W. Wilson, Phys. Rev. C **20**, 2267 (1979).
- [12] J. I. Kapusta and Y. Li, arXiv:nucl-th/0503075.
- [13] T. Csörgő and B. Lörstad, Phys. Rev. C **54**, 1390 (1996)
- [14] U. Heinz, in: *Correlations and Clustering Phenomena in Subatomic Physics*, edited by M.N. Harakeh, O. Scholten, and J.H. Koch, NATO ASI Series B, (Plenum, New York, 1997) (Los Alamos eprint archive nucl-th/9609029)
- [15] B. Tomasik and U. W. Heinz, Eur. Phys. J. C **4**, 327 (1998) [arXiv:nucl-th/9707001].
- [16] F. Cooper and G. Frye, Phys. Rev. D **10**, 186 (1974).
- [17] U.A. Wiedemann, P. Scotto and U. Heinz, Phys. Rev. C **53**, 918 (1996)
- [18] F. Retiere and M. A. Lisa, Phys. Rev. C **70**, 044907 (2004)
- [19] L. S. Kisslinger Phys. Rev. **98**, 761 (1955)
- [20] M. Csanad, T. Csörgő, B. Lorstad and A. Ster, J. Phys. G **30**, S1079 (2004); T. Csörgő and B. Lorstad, Phys. Rev. C **54**, 1390 (1996); M. Csanad, T. Csörgő and B. Lorstad, Nucl. Phys. A **742**, 80 (2004).
- [21] J. Adams, *et al.* [STAR Collaboration], Phys. Rev. C (submitted for publication, 2004);nucl-ex/0411036
- [22] J. Adams, *et al.* [STAR Collaboration], Phys. Rev. Lett. **92**, 112301 (2004).
- [23] S. V. Akkelin and Y. M. Sinyukov, arXiv:nucl-th/0310036.
- [24] B. B. Back *et al.*, Phys. Rev. C **70**, 051901 (2004).
- [25] Yale University, Ph.D. Thesis 2001 “Measurement of Jets and Jet Quenching at RHIC”
- [26] C. W. De Jager, H. De Vries and C. De Vries, Atom. Data Nucl. Data Tabl. **36**, 495 (1987).
- [27] S. Chapman, P. Scotto and U. W. Heinz, Phys. Rev. Lett. **74**, 4400 (1995).
- [28] H. Heiselberg and A. P. Vischer, Eur. Phys. J. C **1**, 593 (1998).
- [29] M. C. Chu, S. Gardner, T. Matsui and R. Seki, Phys. Rev. C **50**, 3079 (1994) [arXiv:nucl-th/9408005].
- [30] B. Tomasik and U. W. Heinz, arXiv:nucl-th/9805016.
- [31] C. Y. Wong, J. Phys. G **29**, 2151 (2003).
- [32] G. E. Brown and M. Rho, Phys. Rev. Lett. **66**, 2720 (1991).
- [33] V. Koch, *Prepared for International Summer School on Correlations and Clustering Phenomena in Subatomic Physics, Dronten, Netherlands, 5-16 Aug 1996* V. Koch, Int. J. Mod. Phys. E **6**, 203 (1997).
- [34] D. T. Son and M. A. Stephanov, Phys. Rev. D **66**, 076011 (2002) D. T. Son and M. A. Stephanov, Phys. Rev. Lett. **88**, 202302 (2002)
- [35] D. Boyanovsky, H. J. de Vega and S. Y. Wang, Nucl. Phys. A **741**, 323 (2004).
- [36] G. A. Baker, B. G. Nickel and D. I. Meiron, Phys. Rev. B **17**, 1365 (1978).
- [37] C. Sasaki, Prog. Theor. Phys. Suppl. **156**, 174 (2004)